USE OF POLYACRYLONITRILE AS ANODIC ARTIFICIAL SOLID ELECTROLYTE INTERPHASE
FOR AQUEOUS-BASED ZINC-ION BATTERIES

Miss Nutchaya Muangplod

A Thesis Submitted in Partial Fulfillment of the Requirements
for the Degree of Master of Engineering in Chemical Engineering
Department of Chemical Engineering
FACULTY OF ENGINEERING
Chulalongkorn University
Academic Year 2021
Copyright of Chulalongkorn University

การใช้พอลิอะคริโลไนไตรล์เป็นชั้นอินเทอร์เฟสอิเล็กโทรไลต์ของแข็งเทียมบนขั้วแอโนด
ในแบตเตอรี่ไอออนสังกะสีฐานน้ำ

น.ส.ณัฐชยา ม่วงปลอด

วิทยานิพนธ์นี้เป็นส่วนหนึ่งของการศึกษาตามหลักสูตรปริญญาวิศวกรรมศาสตรมหาบัณฑิต
สาขาวิชาวิศวกรรมเคมี ภาควิชาวิศวกรรมเคมี
คณะวิศวกรรมศาสตร์ จุฬาลงกรณ์มหาวิทยาลัย
ปีการศึกษา 2564
ลิขสิทธิ์ของจุฬาลงกรณ์มหาวิทยาลัย

Thesis Title	USE OF POLYACRYLONITRILE AS ANODIC ARTIFICIAL SOLID ELECTROLYTE INTERPHASE FOR AQUEOUS-BASED ZINC-ION BATTERIES
By	Miss Nutchaya Muangplod
Field of Study	Chemical Engineering
Thesis Advisor	Professor ANONGNAT SOMWANGTHANAROJ, Ph.D.
Thesis Co Advisor	Associate Professor SOORATHEP KHEAWHOM, Ph.D.

Accepted by the FACULTY OF ENGINEERING, Chulalongkorn University in Partial Fulfillment of the Requirement for the Master of Engineering

.... Dean of the FACULTY OF ENGINEERING

(Professor SUPOT TEACHAVORASINSKUN, D.Eng.)

THESIS COMMITTEE

.... Chairman

(Assistant Professor SUPHOT PHATANASRI, Ph.D.)

.... Thesis Advisor

(Professor ANONGNAT SOMWANGTHANAROJ, Ph.D.)

.... Thesis Co-Advisor

(Associate Professor SOORATHEP KHEAWHOM, Ph.D.)

.... Examiner

(Assistant Professor PIMPORN PONPESH, Ph.D.)

.... External Examiner

(Assistant Professor Pornchai Bumroongsri, D.Eng.)

ณัฐชยา ม่วงปลอด : การใช้พอลิอะคริโลไนไตรล์เป็นชั้นอินเทอร์เฟสอิเล็กโทรไลต์ของแข็งเทียมบนขั้วแอโนดในแบตเตอรี่ไอออนสังกะสีฐานน้ำ. (USE OF POLYACRYLONITRILE AS ANODIC ARTIFICIAL SOLID ELECTROLYTE INTERPHASE FOR AQUEOUS-BASED ZINC-ION BATTERIES) อ.ที่ปรึกษาหลัก : ศ. ดร.อนงค์นาฏ สมหวังธนโรจน์, อ.ที่ปรึกษาร่วม : รศ. ดร.สุรเทพ เขียวหอม

แบตเตอรี่ไอออนสังกะสีฐานน้ำแบบชาร์จซ้ำได้นั้นเป็นที่น่าสนใจในการนำมาทำระบบกักเก็บพลังงาน เนื่องจากความจุเฉพาะสูง, ต้นทุนต่ำ และความปลอดภัย อย่างไรก็ตามในการใช้งานจริงของแอโนดสังกะสีในอิเล็กโทรไลต์ที่เป็นกรดอ่อนๆ ถูกจำกัดด้วยปัญหาหลายประการ เช่น การเกิดเดนไดรต์, การกัดกร่อน, การเกิดก๊าซไฮโดรเจน, การเกิดชั้นฟิล์ม และประสิทธิภาพวงรอบการอัดคายประจุของแบตเตอรี่ที่ค่อนข้างต่ำ การเคลือบแอโนดสังกะสีด้วยแกรไฟต์ (GP) (GP@Zn) สามารถแก้ปัญหาเหล่านี้ได้บางส่วนและสามารถปรับปรุงประสิทธิภาพวงรอบการอัดคายประจุของแบตเตอรี่ได้ อย่างไรก็ตามหลังจากรอบการชาร์จ/การคายประจุเป็นเวลานาน สังกะสีมีแนวโน้มที่จะย้ายตำแหน่งและสะสมซ้ำบนพื้นผิวของแกรไฟต์ เนื่องจากค่าการนำไฟฟ้าของอนุภาคแกรไฟต์ ดังนั้นหลังจากการอัดคายประจุเป็นเวลานาน ปัญหาดังกล่าวจึงกลับมา การสร้างชั้นอินเทอร์เฟสอิเล็กโทรไลต์ของแข็งเทียม (ASEI) บนพื้นผิวของแอโนดสังกะสีมีแนวโน้มที่จะสามารถแก้ปัญหานี้ได้ ซึ่งในงานนี้ใช้พอลิอะคริโลไนไตรล์ (PAN) กับซิงค์ไตรฟลูออโรมีเทนซัลโฟเนต ($Zn(CF_3SO_3)_2$) (PANZ) เป็นชั้น ASEI ที่ถูกเคลือบบนชั้นแกรไฟต์บนแอโนดสังกะสี (PANZ@GP@Zn) โดยเปรียบเทียบกับแอโนดที่มีชั้นเคลือบด้วยแกรไฟต์และแอโนดสังกะสีเปล่า ชั้นเคลือบถูกเตรียมโดยวิธีด็อกเตอร์เบลด ผลการวิจัยแสดงให้เห็นว่าแอโนดที่มีการเคลือบด้วยชั้นพอลิอะคริโลไนไตรล์กับซิงค์ไตรฟลูออโรมีเทนซัลโฟเนตบนชั้นแกรไฟต์สามารถลดการสะสมของสังกะสีบนผิวของแอโนดได้ เมื่อเปรียบเทียบกับแอโนดที่มีการเคลือบชั้นแกรไฟต์ นำไปสู่ความเสถียรของวงรอบการอัดคายประจุของแบตเตอรี่สูงและยืดอายุการใช้งานของแบตเตอรี่

สาขาวิชา	วิศวกรรมเคมี	ลายมือชื่อนิสิต ....
ปีการศึกษา	2564	ลายมือชื่อ อ.ที่ปรึกษาหลัก ....
		ลายมือชื่อ อ.ที่ปรึกษาร่วม ....

6370089921 : MAJOR CHEMICAL ENGINEERING

KEYWORD: Rechargeable aqueous zinc-ion batteries, Zinc anode, Polyacrylonitrile

Nutchaya Muangplod : USE OF POLYACRYLONITRILE AS ANODIC ARTIFICIAL SOLID ELECTROLYTE INTERPHASE FOR AQUEOUS-BASED ZINC-ION BATTERIES. Advisor: Prof. ANONGNAT SOMWANGTHANAROJ, Ph.D. Co-advisor: Assoc. Prof. SOORATHEP KHEAWHOM, Ph.D.

Rechargeable aqueous zinc-ion batteries (ZIBs) have attracted attention for energy storage systems because of their high specific capacity, low cost, and safety. However, practical application of the zinc anode in mild acidic electrolytes is limited by several issues such as dendrite formation, corrosion, hydrogen evolution reaction, passivation and relatively low cycling performance. Coating the zinc anode with graphite (GP) (GP@Zn) can partially solve these issues and improves the cycling performance of ZIB. However, after long-term charge/discharge cycles, zinc tends to migrate and redeposit over the surface of GP owing to the electronic conductivity of GP particles. Thus, after long-term cycling, the issues mentioned are back. Fabrication of artificial solid electrolyte interphase (ASEI) on the surface of the zinc anode shows high potential for solving these issues. In this work, polyacrylonitrile (PAN) with zinc trifluoromethanesulfonate ($Zn(CF_3SO_3)_2$) (PANZ) as ASEI was coated on the GP layer onto the zinc anode (PANZ@GP@Zn), and compared with the anode having GP coated layers and pristine zinc anode. The coating layer was prepared by the doctor blading method. The result showed that the PANZ@GP@Zn anode can reduce zinc deposition over the anode surface when compared with the GP@Zn anode, leading to the high cycling stability of ZIBs and extending the battery's life.

Field of Study: Chemical Engineering   Student's Signature ....

Academic Year: 2021   Advisor's Signature ....

Co-advisor's Signature ....

ACKNOWLEDGEMENTS

TABLE OF CONTENTS

LIST OF TABLES

LIST OF FIGURES

จุฬาลงกรณ์มหาวิทยาลัย
CHULALONGKORN UNIVERSITY

Chapter I

Introduction

1.1 Introduction

The demand for renewable energy has risen rapidly due to fossil fuels over-consumption and environmental pollution and global warming issues. However, renewable energy is difficult to store, transport and its fluctuating nature. Therefore, an energy storage system (ESS) has been developed to provide a more versatile and stable power supply for personal, household and industrial applications [1].

The most well-studied energy storage system and widely used in the energy market is lithium-ion batteries (LIBs), which can provide high energy density, and long cycle lifetime [2]. Nonetheless, commercial LIBs are still suffered from high cost due to the limited lithium resource and safety issues, also hinder their development for large-scale energy storage applications. Considering these limitations of LIBs, it is necessary to search for new battery technology based on high safety, low cost, and long cycle life [3].

Rechargeable aqueous zinc-ion batteries (ZIBs) have been considered as the promising alternative energy storage system to the currently due to their high theoretical capacity (820 mAh g^{-1}), natural abundance, low cost, environmental friendliness, and high safety [4]. However, the practical application of the zinc anode in mildly acidic electrolytes is limited by several issues such as dendrite formation, corrosion, hydrogen evolution, passivation on the zinc surface, which reduces coulombic efficiency and cycling performance of ZIBs [1], [4] .

One of various carbon materials that is a good alternative for using in zinc anodes is graphite (GP) due to its homogeneous electric field distribution, abundant active sites, and satisfying durability, leading to the enhancement on the cycling performance of ZIBs [5], [6], [7]. Hence, coating the zinc anode with graphite can

partially solve these issues. However, after long-term charge/discharge cycles, zinc tends to migrate and redeposit over the surface of the carbon layer owing to a good electronic conductivity of carbon particles [3]. Thus, after long-term cycling, the mentioned issues are back.

Polyacrylonitrile (PAN) is a solid polymer electrolyte that is attractive for use in ZIBs due to its low cost, chemical stability, excellent thermal stability, high tensile strength and tensile modulus. The polar nitrile group (-CN) can provide coordination sites to bridge Zn^{2+} ions. Nevertheless, polyacrylonitrile has partially hydrophobicity (ionic conductivity $\sim10^{-4}$ S cm^{-1}), so it is improved by adding zinc trifluoromethane-sulfonate ($Zn(CF_3SO_3)_2$) or ($Zn(TfO)_2$) to this polymer to increase its hydrophilicity and higher ionic conductivity [8]. Also, The S–O$^-$ anions of $Zn(CF_3SO_3)_2$ can react with Zn^{2+} ions [9]. Hence, Polyacrylonitrile with zinc trifluoromethanesulfonate are used as artificial solid electrolyte interphase (ASEI) on the surface of the zinc anode that can regulate zinc ion distribution and uniform nucleation sites for zinc deposition on the anode surface [10]. Thus, ASEI shows high potential for solving the problem that zinc tends to migrate and redeposit over the surface of carbon.

In this study, polyacrylonitrile (PAN) with zinc trifluoromethanesulfonate ($Zn(CF_3SO_3)_2$) (PANZ) as ASEI was coated on the graphite (GP) layer onto the zinc anode (PANZ@GP@Zn), and the results were compared to the anode having graphite coated layers and bare zinc anode in rechargeable aqueous zinc-ion batteries.

1.2 Objective

1. Develop a zinc anode coating layer to solve the carbon layer problem.
2. To suppress side reactions of zinc anode in a mildly acidic electrolyte leading to high cycling stability of ZIBs.

1.3 Scope of research

1. The anode was prepared by using polyacrylonitrile (PAN) with zinc trifluoromethane sulfonate ($Zn(CF_3SO_3)_2$) (PANZ) as artificial solid electrolyte interphase (ASEI) which was coated on the graphite (GP) layer onto zinc foil.

2. The weight ratio of graphite:polyvinylidene fluoride (PVDF) as a binder is 80:20.

3. Glass microfiber paper as a separator.

4. The cathode was δ-MnO_2.

5. The electrolyte in batteries was 2 M $ZnSO_4$ used in symmetrical cell and 2 M $ZnSO_4$ + 0.5 M $MnSO_4$ used in full cell.

6. The batteries were fabricated as CR2025 cell and measured by a three-electrode setup to inspect electrochemical performance.

1.4 Research plan

Table 1 Research plan 1

Activities	Period											
	2021						2022					
	Jul	Aug	Sep	Oct	Nov	Dec	Jan	Feb	Mar	Apr	May	Jun
1. Literature survey and overview of the zinc anode and ZIBs.	■	■	■	■								
2. Develop coating layer of zinc anode.				■	■	■	■	■	■	■	■	
3. Test batteries performance and characterization of batteries.						■	■	■	■	■	■	■
4. Analyze experiment result.							■	■	■	■	■	■
5. Write thesis and publication.							■	■	■	■	■	■

Chapter II

Theory and Literature review

2.1 Zinc-ion batteries

2.1.1 Overview

Zinc ions react at both electrodes and move between them through a water-based electrolyte in a zinc-ion battery. Zinc metal at the anode is dissolved into the electrolyte as zinc ions during discharge. The cathode absorbs zinc ions from the electrolyte at the same time. This process is reversed during charge that is illustrated in Figure 2.1.
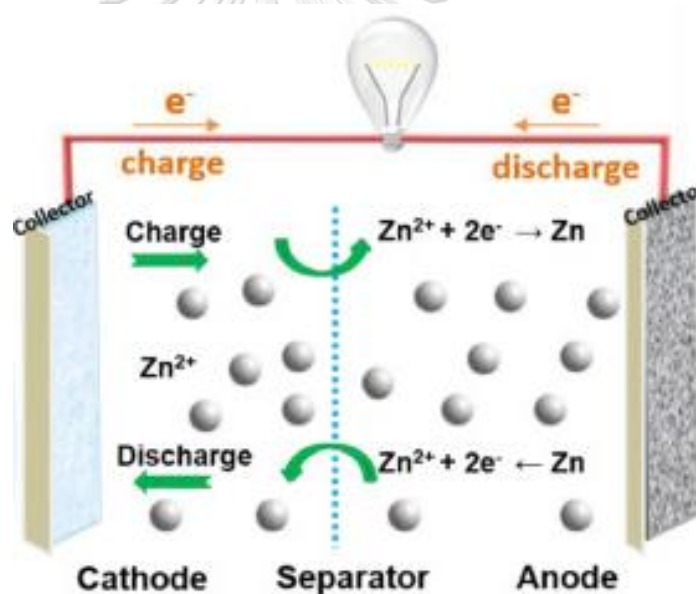
Figure 2.1 Schematic illustration of ZIBs. [11]

Rechargeable aqueous zinc-ion batteries (ZIBs) utilizing zinc (Zn) as the anode in a mildly acidic electrolyte have attracted attention because heavy Zn dendrites formation and passivating byproducts (e.g. ZnO and $Zn(OH)_2$) in an alkaline electrolyte is considerably reduced on Zn anode in a mildly acidic electrolyte. However, problems with critical concerns in the Zn metal anode in a mildly acidic electrolyte have been discovered in the practical application of ZIBs [4].

2.1.2 Side reactions on the anode surface

The charging/discharging processes of ZIBs are accompanied by the reversible plating/stripping of Zn^{2+} ions on the anode surface in a mildly acidic electrolyte. The reaction mechanisms of the Zn anode are displayed as expressed in equation 2.1 and 2.2:

$$\text{Stripping (discharge process): } Zn_{(s)} \longrightarrow Zn^{2+}_{(aq)} + 2e^- \quad \text{(eq.2.1)}$$

$$\text{Plating (charge process): } \quad Zn^{2+}_{(aq)} + 2e^- \longrightarrow Zn_{(s)} \quad \text{(eq.2.2)}$$
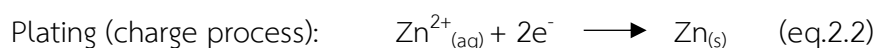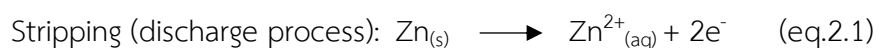
Zn has a high electrochemical activity and thermodynamical instability in mild aqueous electrolytes during the reversible plating/stripping process, resulting in side reactions of Zn anode such as dendrite formation, corrosion, hydrogen evolution and passivation as shown in Figure 2.2, leading to low coulombic efficiency and cycling performance of ZIBs [12].
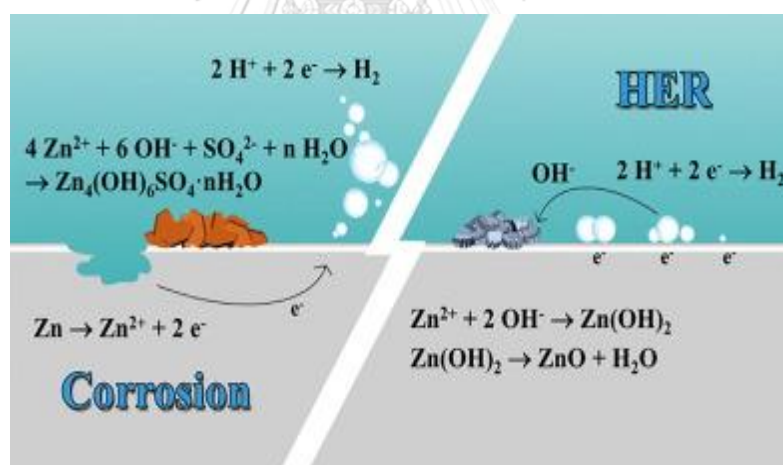
Figure 2.2 The fundamentals of side reactions of Zn anodes in a mildly acidic electrolyte. [4]

2.1.2.1 Dendrite formation

Uneven Zn deposition during the charging process which results in Zn dendrites formation. Zinc ions absorbed on the surface diffuse in two directions along the surface, forming protrusions at priority nucleation sites (dendrite) [3], when

large dendrites may penetrate through the separator, which causes a short circuit in the batteries. In addition, "dead Zn" can occur when flake-like Zn dendrites fall off the electrode due to the loose structure that is illustrated in Figure 2.3. As a result, the coulombic efficiency and battery lifespan are reduced [12].
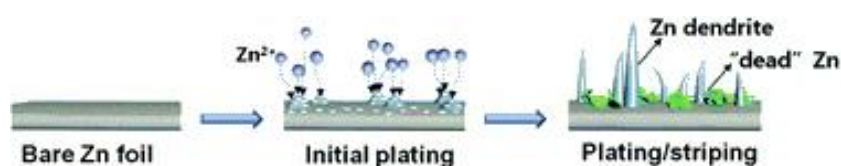
Figure 2.3 Schematic illustration of Zn deposition on bare Zn and the formation of Zn dendrite. [13]

2.1.2.2 Hydrogen evolution reactions (HER)

The hydrogen evolution reaction (HER) is caused by water that is primary side reaction. However, the hydrogen evolution at the anode in a mildly acidic electrolyte occurs during the battery's rest and operation. Hence, the standard reduction potential of Zn/Zn^{2+} (–0.76 V vs SHE) has a lower redox potential than hydrogen evolution potential (0 V vs SHE) and Zn tends to react with water and release hydrogen bubble gas, leading to HER in a neutral or mildly acidic aqueous ZIB electrolyte. Their reaction mechanisms are displayed as expressed in equation 2.3 and 2.4. During the charging process, hydrogen accumulates in the battery, causing it to expand owing to increase internal pressure until it explodes and electrolyte leakage. As a result, HER in a mildly acidic aqueous ZIB electrolyte can irreversibly consume electrodes and electrolytes, resulting in reduced battery life and CE. [1], [3], [12].

$$Zn \longleftrightarrow Zn^{2+} + 2e^- \qquad \text{(–0.76 V vs. SHE)} \qquad \text{(eq.2.3)}$$

$$2H^+ + 2e^- \longleftrightarrow H_2 \qquad \text{(0 V vs. SHE)} \qquad \text{(eq.2.4)}$$

2.1.2.3 Corrosion reactions (hydrogen evolution and passivation)

Corrosion in mild systems is inseparable from HER, so electrochemical corrosion is also a difficult problem and a critical problem in the development of ZIBs. In a neutral electrolyte, Zn metal corrodes relatively slowly. The corrosion process will be accelerated by Zn metal in a mild acid electrolyte. During battery resting, the corrosion site at the interface of Zn metal-electrolyte can occur which caused by Zn dissolution (anodic process) due to the loss of electrons as expressed in equation 2.5 [4], [12].

Zn dissolution (anodic process): $\quad$ $Zn \longrightarrow Zn^{2+} + 2e^-$ $\qquad$ (eq.2.5)

The released electrons are accepted by electron acceptors in the electrolyte such as a proton (H^+), a water molecule (H_2O). Hence, a proton is accepted electrons to generate hydrogen gas (H_2 gas generation reaction: HER) as expressed in equation 2.6.

H_2 gas generation reaction (cathodic process): $\ 2H^+ + 2e^- \longrightarrow H_2$ $\quad$ (eq.2.6)

Corrosion in a mildly acidic electrolyte occurs equation (2.5) and (2.6), which are accompanied with the precipitation of complicated Zn as corrosion products (passivation) caused by when H^+ is consumed in water, residual OH^- ions accumulate along the interface of anode-electrolyte, react with Zn^{2+} cations and other electrolyte components to form by-products or corrosion products on the anode surface [1], [4]. However, different types of electrolytes and operating environments may have different by-products. In mildly acidic electrolyte such as $ZnSO_4$ electrolyte can form $Zn(OH)_2$ and $Zn_4SO_4(OH)_6 \cdot nH_2O$ with a hexagonal structure on anode surface as expressed in equation 2.7 [12]. Thus, corrosion products or passivation causes the low plating/stripping coulombic efficiency (CE) and the performance of the battery [3] , [12].

$4Zn^{2+} + SO_4^{2-} + 6OH^- + nH_2O \longrightarrow Zn_4(OH)_6SO_4 \cdot nH_2O$ $\qquad$ (eq.2.7)

Dendrite formation, hydrogen evolution, and corrosion are all linked. The growth of dendrites results in a porous anode structure, which increases the contact surface between the electrode and the electrolyte and reduces the current density, resulting in additional reaction sites for accelerated HER and corrosion. Also, the increasing of hydrogen bubbles on the anode surface can prevent Zn nucleation, leading to increased overpotential and uneven Zn deposition. On the one hand, forming nonconductive byproducts that hinder the electron transport [1], [12].

2.2 Coating layer

2.2.1 Carbon materials

In rechargeable Zinc-ion batteries, anode has developed for suppressing side reactions on the anode surface, which is required to increase battery performance. Carbon materials are used widely in ZIBs with its advantages such as high conductivity, high chemical stability, low price, and non-toxicity. Hence, carbon materials have received a lot of interest as a way of solving anode problems [6], [14].

From Li et. al. research, [5], activated carbon (AC) coated on Zn anode (Zn@C) has developed for the long-term cycle stability of batteries. Figure 2.4a shows the fluctuation of the Zn symmetrical cell's cycling curves at a current density of 1 mA cm^{-2} because inhomogeneous current distribution caused by surface morphological change during stripping/plating. In contrast, The Zn@C symmetrical cell exhibits more stable cycling, indicating that Zn@C undergoes lower morphological change.
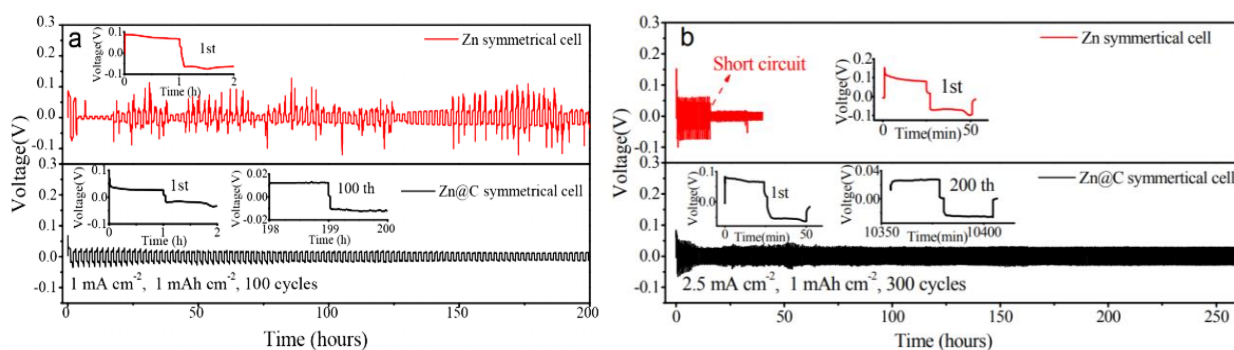
Figure 2.4 Stripping/plating performance o of Zn and Zn@C cells at (a) 1 and (b) 2.5 mA cm⁻² with 1 mAh cm⁻². [5]

The Zn@C symmetrical cell shows stable cycling above 300 cycles (>250 h) when current density is increased to 2.5 mA cm^{-2}, whereas the Zn symmetrical cell (bare Zn) can only last a few hours before short circuiting, as illustrated in Figure 2.4b. The Zn@C symmetrical cell can run for 100 hours with an overpotential of less than 0.1 V even at higher current densities of 5 and 10 mA cm^{-2}. As a result, a Zn anode (Zn@C) coated with activated carbon (AC) provides stable Zn stripping/plating.
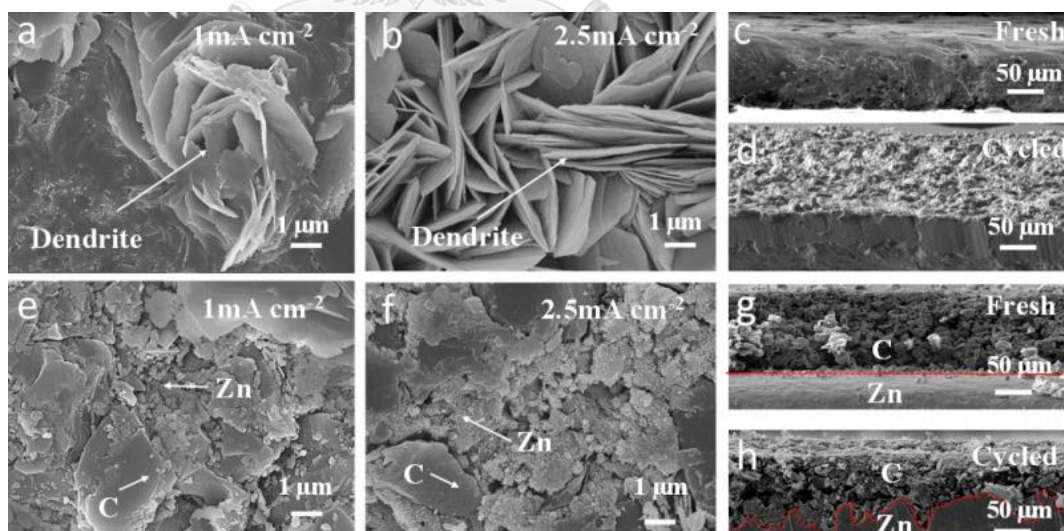
Figure 2.5 Top-view SEM images of Zn and Zn@C electrode cycled at 1 and 2.5 mA cm⁻² and cross-section view SEM images of fresh and cycled of fresh Zn and Zn@C electrode at 2.5 mA cm⁻² . [5]

At 1 and 2.5 mAcm^{-2}, the morphology of Zn@C after continuous plating/stripping is non-dendrite, owing to the increased surface area of the carbon film, which adsorbs and causes Zn to preferentially fill the spaces between carbon particles in a sphere shape rather than perpendicular growth, which suppresses Zn dendrite formation, as shown in Figure 2.5e, f. As illustrated in Figure 2.5h, Zn ions are deposited mostly at the interface between the Zn and carbon layers, as well as within the carbon layer itself (inner space and surface voids). Thus, activated carbon (AC) was coated on Zn anode (Zn@C), which provides the long-term cycle stability of batteries and inhibits Zn dendrite formation because the porous carbon layer facilitating homogeneous current distribution and Zn deposition.

From Li, Z. et. al., 2020, [7], the graphite layer was painted directly onto the anode surface by using regular pencils to investigate dendrite-free feature and cycling performance of the battery. In comparison to certain metals and inorganic materials, graphite has lower Young's modulus (27 GPa), which gives it an advantage for Zn modification (Figure 2.6f). This unique feature gives graphite high ductility and compressibility, which suggests that the Zn-G anode might show good durability as a result of this flexible interlayer.
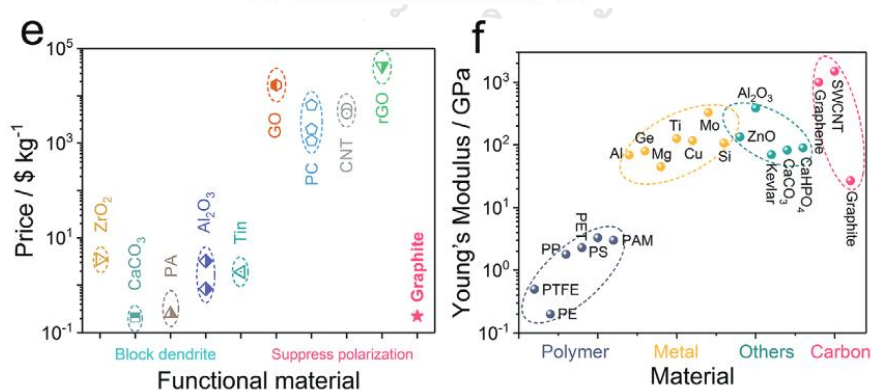
Figure 2.6 (e) Cost comparison of graphite with other reported functional materials. (f) Young's modulus comparison of various materials. [7]

After soaking in 2 M ZnSO$_4$ solution for 15 days, the pristine Zn surface was seriously oxidized together with an obvious color change (from silver to gray). However, the Zn–G electrode still holds a stable surface without obvious byproducts after 15 days as shown in Figure 2.7.

Figure 2.7 Schematic illustration of the modification process and the stability in 2 M ZnSO$_4$ electrolyte of Zn and Zn–G anodes. [7]
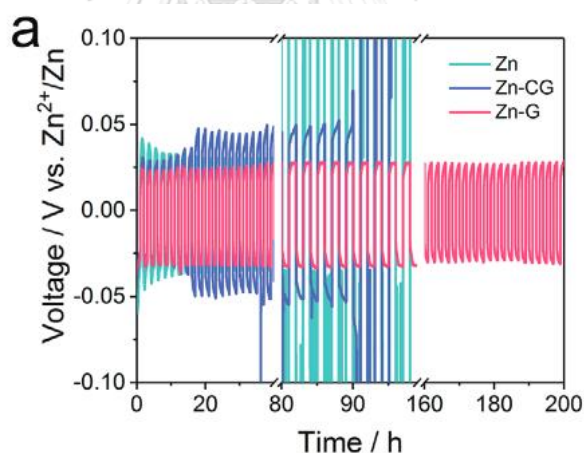
Figure 2.8 Electrochemical stability of the Zn, Zn-CG and Zn-G cells at current density of 0.1 mA cm^{-2} with capacity of 0.1 mAh cm^{-2}. [7]

The electrochemical stability of the Zn and Zn–G anodes was evaluated in 2 M ZnSO$_4$ by the repeated galvanostatic test of symmetric cells at current density of 0.1 mA cm^{-2} with capacity of 0.1 mAh cm^{-2} as shown in Figure 2.8. Compared to the Zn-CG‖Zn-CG cell (modified by commercial graphite), the Zn‖Zn cells fail rapidly with

an obvious voltage increase after ≈70 and ≈90 h plating/stripping, respectively, which is probably caused by the dendrite-induced internal short circuit. Moreover, the initial and last cycles further confirm the superior stability of Zn–G anode.
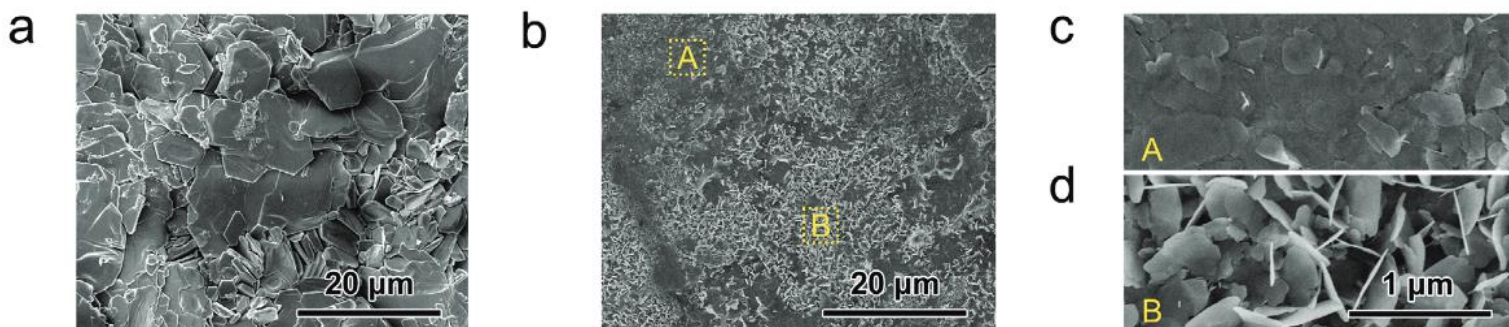
Figure 2.9 SEM images of a) Zn and b–d) Zn–G electrodes after cycling 24 h with the capacity of 1.5 mAh cm^{-2}. [7]

To study the morphology of the bare Zn and Zn–G anodes by SEM. After deposition with relatively high capacity of 1.5 mAh cm^{-2}, the Zn was deposited into uneven huge blocks by numerous aggregated nanosheets (Figure 2.9a), leading to dendrites growth and short circuit of battery. In contrast, Zn is uniformly deposited and filled into the coated graphite layer on the surface of Zn-G without the formation of dendrites (Figure 2.9b, c). With the continuous plating of Zn, a well-defined array structure can be formed by 2D nanosheet (Figure 2.9b, 2.9d).
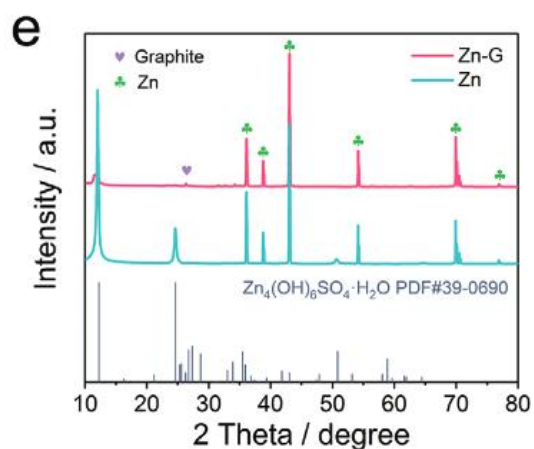
Figure 2.10 XRD patterns of Zn and Zn–G after cycling tests. [7]

The bare Zn anode, as shown in Figure 2.10e, displays some new sharp peaks at 12.1, 24.6, and 50.7 degrees, which are well attributed to the $Zn_4(OH)_6SO_4H_2O$. This byproduct was mostly created when Zn was plated and stripped in an aqueous $ZnSO_4$ electrolyte. However, the cycled Zn-G electrode shows only exhibits one characteristic peak of such a byproduct at 12.1°. Compared to the surface of bare Zn cell, the Zn-G cell exhibits less byproducts, which is the uniform electric field and highly reversible processes during repeated cycling, while the bare Zn anode found continuous formation of this byproduct during noncomplete reversible plating/ stripping, leading to a short lifespan and even the batteries' failure.
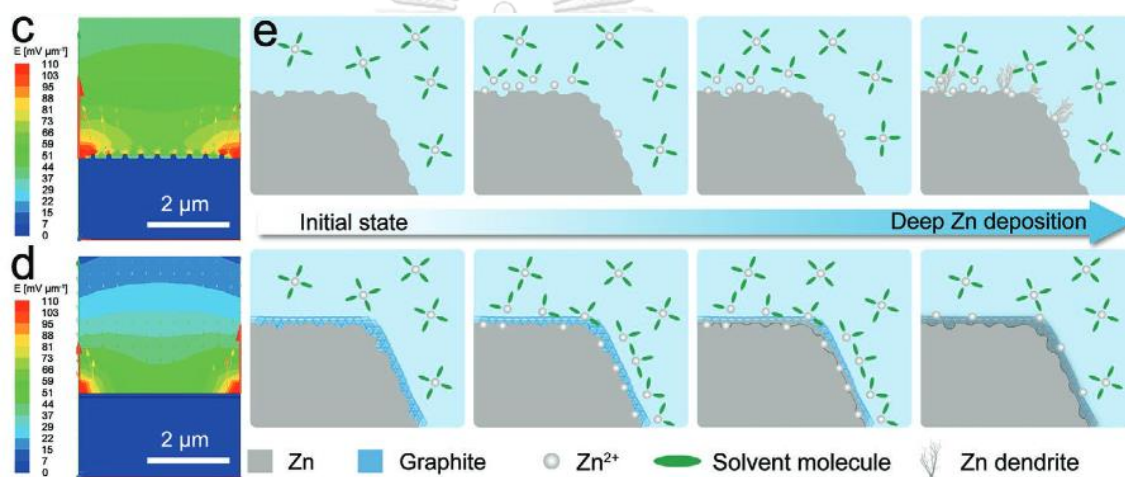
Figure 2.11 The electric field distributions for c) Zn and d) Zn–G electrodes. e) Brief illustration of Zn deposition on Zn and Zn–G electrodes. [7]

Additionally, Ansoft Maxwell software was used to simulate the electric field distributions for both electrodes after Zn deposition in order to determine how the graphite functional layer can result in dendrite-free plating. Figure 2.11c shows that the distribution of electric fields is not uniform, particularly at the tips of dendrites and the edges of Zn. As a result of the high intensity gradient, more Zn^{2+} ions are likely to adsorb and form nuclei at these locations, leading to even more unequal deposition and the formation of dendrites. Importantly, the Zn-G only exhibits a relatively homogenous electric field distribution after the addition of a soft layer of

graphite (Figure 2.11d). The Zn nuclei size can be decreased by its low the nucleation overpotential (NOP) and uniformly deposited procedure will be performed caused by the strong conductivity, low Young's modulus, and large voids in graphite. These results also reveal that more Zn^{2+} ions can initially deposit in the layer space of graphite and adsorbed onto the entire electrode surface. Due to its soft interfaces, the Zn-G still exhibits great reversibility and dendrite-free characteristics over long-term cycling (Figure 2.11e). Owing to the unique physiochemical features, the Zn-G may comprehensively efficiently limit the effects of dendrites or other passivation byproducts, favoring the reversible and stable electrochemical behaviors.

Thus, a graphite-based functional interface has been performed to engineer a durable Zn anode by directly drawing with a common pencil. Due to the high conductivity, low Young's modulus, and porosity of graphite, the soft interface endows Zn anode with low NOP, homogeneous electric field distribution, abundant active sites, and satisfying durability. As a result, the Zn–G anode shows remarkably enhanced durability over 200 h and dendrite-free feature, much better than that for bare Zn anode.

From Li, C. et. al. work in 2020, [3], the problem of the carbon coating layer is after long-term charge/discharge cycles, zinc tends to migrate and redeposit over the surface of carbon owing to a good electronic conductivity of carbon particles. Thus, after long-term cycling, the side reactions were still found on carbon coating layer surface.

2.2.2 Artificial solid electrolyte interphase (ASEI)

From Chen, P. et. al. work in 2020, [8], polyacrylonitrile (PAN) is a solid polymer electrolyte that is attractive for use in ZIBs due to its low cost, chemical stability, excellent thermal stability, high tensile strength and tensile modulus, which

can adjust to volume changes during metal plating/stripping. As a result, the mechanical flexibility of the PAN film also limits uncontrollable zinc deposition [8]. The polar nitrile group (-CN) provides coordination sites to bridge Zn^{2+} ions [9].
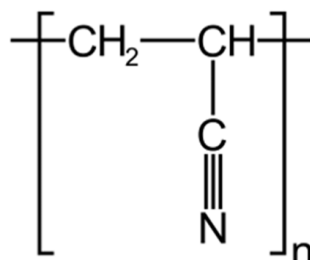
Figure 2.12 Molecular structure of polyacrylonitrile [15]

Nevertheless, polyacrylonitrile has partially hydrophobicity (ionic conductivity ~10^{-4} S cm^{-1}), so it is improved by adding zinc trifluoromethanesulfonate ($Zn(CF_3SO_3)_2$) or ($Zn(TfO)_2$) to this polymer to increase ionic conductivity [8] as shown in Figure 2.13. Also, The S–O$^-$ anions of $Zn(CF_3SO_3)_2$ can react with Zn^{2+} ions [10].
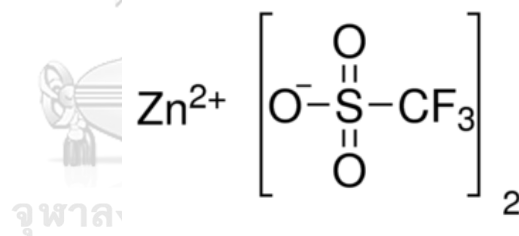
Figure 2.13 Molecular structure of zinc trifluoromethanesulfonate [16]
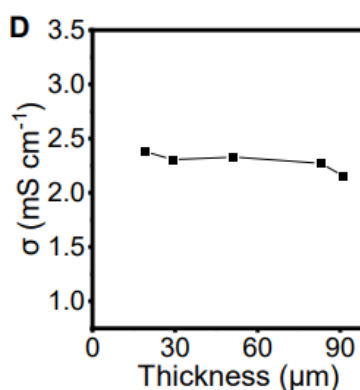
Figure 2.14 Ionic conductivity of PANZ membranes with varying thickness [8]

Hence, Polyacrylonitrile with zinc trifluoromethanesulfonate are used as artificial solid electrolyte interphase (ASEI) on the surface of the zinc anode, which can regulate zinc ion distribution and uniform nucleation sites for Zn deposition on the anode surface.

Chapter III

Experiments

3.1 Materials

Graphite (GP) powder, <20 μm was purchased from Sigma-Aldrich, polyacrylonitrile (PAN) (MW. 150,000 g/mol) was purchased from Sigma-Aldrich, zinc trifluoromethanesulfonate ($Zn(CF_3SO_3)_2$) was purchased from Sigma-Aldrich, n,n-dimethyl formamide 99.8% (AR/ACS grade) (DMF) was purchased from Loba Chemie, n-methylpyrrolidone (AR grade) (NMP) was purchased from Quality reagent chemicals, poly(vinylidene fluoride) (Solef®PVDF) (MW. 180,000 g/mol) was purchased from Solvay, zinc sulfate 7-hydrate ($ZnSO_4 \cdot 7H_2O$) (AR grade, MW 287.58 g/mol) was purchased from Kemaus. Zinc foil (thickness: 0.05 mm), graphite foil (thickness: 0.05 mm), glass microfiber paper (GF/A, Whatman) and blank coin cell CR2025 were used as received.

3.2 Preparation of CR2025 battery type

3.2.1 Anode preparation

3.2.1.1 Preparation of graphite coated Zn foil (GP@Zn)

The graphite was mixed with polyvinylidene fluoride (PVDF) in n-methylpyrrolidone (NMP) solution with the weight ratio of carbon:PVDF as a binder was 80:20, that was prepared under stirring at room temperature until homogeneous. It was then pressed onto a Zn foil (thickness, 50 μm) by the doctor blading method, and dried at 80 °C for overnight in vacuum to evaporate the solvent. The graphite coated Zn foil was rolled with thickness 0.14 mm by battery roller machine. The thickness of the carbon coating layer was 90 μm.

3.2.1.2 Preparation of polyacrylonitrile (PAN) with zinc trifluoromethane-sulfonate ($Zn(CF_3SO_3)_2$) coated graphite layer on Zn foil (PANZ@GP@Zn)

1.0 g of polyacrylonitrile (PAN) was dissolved in 9.0 g dimethylformamide (DMF) under stirring (800 rpm) at 50 °C until the polymer completely dissolved, then 1.0 g zinc trifluoromethanesulfonate ($Zn(CF_3SO_3)_2$) was dissolved in the solution. It was then pressed onto GP@Zn which has been prepared before by the doctor blading method, and dried on the doctor blading machine at 55 °C for 3 h to evaporate the solvent. Finally, anode sheet was obtained and cut into a circular shape with 15 mm in diameter. The thickness of the polymer coating layer was 2-4 µm and 7-9 µm.

3.2.2 Cathode preparation

The δ-MnO_2 was chosen as a cathode for the battery, which was made by dissolving 1.98 g of $KMnO_4$ in 60 mL of deionized (DI) water. Then, $MnSO_4.H_2O$ (0.336 g) was dissolved in 20 mL DI water and dropped into the $KMnO_4$ solution, which had been continuously stirred for 30 minutes. The solution was then transferred to a 100mL Teflon autoclave and heated at 160 °C in an oil bath for 24 hours. The product was collected and cleaned with DI water. It was then dried at 80 °C for 12hr. After   the δ-MnO_2 was obtained then it was mixed with the weight ratio of δ-MnO_2 : super P : PVDF as a binder was 80 : 10 : 10 under stirring until homogeneous. It was pressed onto a graphite (thickness, 50 µm) by the doctor blading method, and dried at 80 °C overnight in vacuum to evaporate the solvent. Finally, cathode sheet was obtained and cut into a circular shape with 15 mm in diameter.

3.2.3 Electrolyte preparation and separator preparation

The electrolyte in batteries was 2 M $ZnSO_4$, and the electrolyte preparation was to dissolve a certain amount of $ZnSO_4$ into DI water under stirring at room temperature until a homogeneous solution was achieved. The separator was a glass microfiber (pore size: 1.2 µm), which was cut into a circular shape with 19 mm in diameter.

3.2.4 Battery Assembly

The batteries were fabricated as a CR2025 coin cell that includes the top cap, spring, spacer, anode, separator, cathode, and bottom cap, respectively, as shown in Figure 3.1. The separator was soaked in 2 M $ZnSO_4$ for 20 minutes while the component was being assembled. A crimping machine was then used to close the cell with a pressure of around 1 ton cm^{-2}.
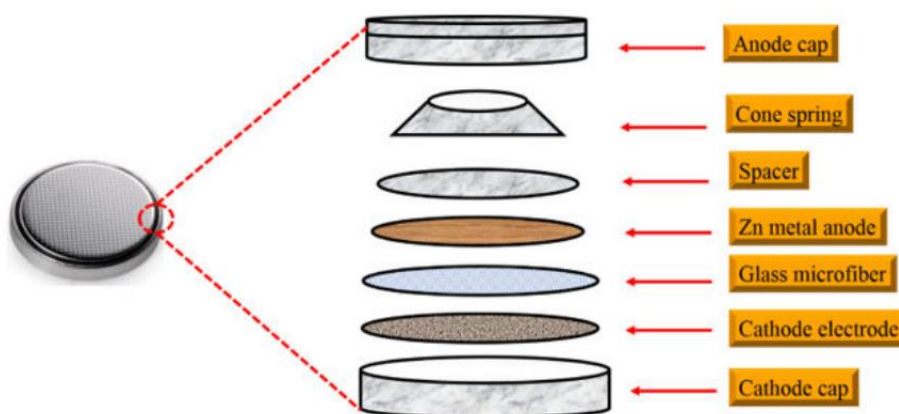
Figure 3.1 The components of a CR2025 coin cell [17]

3.3 Material Characterizations

3.3.1 Field emission scanning electron microscope (FE-SEM)

The field emission scanning electron microscope (FE-SEM) was used to inspect the morphologies of the anode and separator surface both initial and after cycling. The battery was discharged and charged after 100 cycles at current density of 1 mA cm^{-2} with fixed capacity of 1 mAh cm^{-2}. Before FE-SEM analysis, anode was disassembled from the battery and soaked in distilled water for 3 minutes and dried.

3.3.2 Energy-dispersive X-ray spectroscopy (EDS)

Energy-dispersive X-ray spectroscopy (EDS) was used to detect elements found on the anode and separator surface before and after cycling or soaking in 2 M $ZnSO_4$. Before EDS analysis, anode and separator were disassembled from the battery and soaked in distilled water for 3 minutes and dried.

3.4 Electrochemical measurements

3.4.1 Electrochemical impedance spectroscopy (EIS)

EIS measurements were carried out with VersaSTAT tool over the frequency range between 100,000 Hz and 0.1 Hz with an AC voltage of 10 mV. This test was conducted via the potentiometer on three electrodes including bare and coated (bare Zn, GP@Zn and PANZ@GP@Zn) which were the working electrode, zinc foil was counter electrode and Ag/AgCl was reference electrode. The batteries before cycling were observed. The result showed impedance spectra that indicated the electronic and ionic conductivities.

3.4.2 The Tafel curves

The Tafel curves was used to evaluate the corrosion and hydrogen evolution reaction on the anode surface. This test was conducted via the potentiometer on three electrodes including bare and coated (bare Zn, GP@Zn and PANZ@GP@Zn) electrode which were the working electrodes, zinc foil was counter electrode and Ag/AgCl was reference electrode. The Tafel curves of bare Zn, GP@Zn and PANZ@GP@Zn measured in 2 M $ZnSO_4$ at a scan rate of 0.2 mV s^{-1}. The result showed current and potential (vs Zn^{2+}/Zn).

3.4.3 Galvanostatic charge/discharge cycling

The galvanostatic cycling test was the standard method for determination of the cell performance by evaluating the striping/plating performance of bare Zn||bare Zn, GP@Zn||GP@Zn and PANZ@GP@Zn||PANZ@GP@Zn symmetrical cells. The long-term cycling performance and cycling stability of the zinc anodes were measured at a current density of 1 mA cm^{-2} with fixed capacity of 1 mAh cm^{-2}. This method was performed on battery-tester.

3.4.4 The Coulombic efficiency (CE)

The coulombic efficiency (CE) was the percentage of discharging capacity compared with the charging capacity to evaluate the battery's reversibility. The CE of bare and coated zinc (bare Cu||bare Zn, GP@Cu||bare Zn and PANZ@GP@Cu|| bare Zn) were measured at a current density of 1 mA cm^{-2} with fixed capacity of 1 mAh cm^{-2}.

$$Coulombic\ efficiency = \frac{Discharging\ capacity}{Charging\ capacity} \times 100\% \qquad (eq.3.1)$$

3.4.5 Cyclic voltammetry (CV)

Cyclic voltammetry (CV) was analyzed the oxidation and reduction behaviors of batteries. The battery was fabricated as the coin cell in which the anode was Zn foil with bare and coated (bare Zn, GP@Zn and PANZ@GP@Zn) and the cathode was **δ**-MnO$_2$. The CV was measured using VersaSTAT tool and the range of potential between 1 V and 1.8 V, with a scan rate of 0.3 mV s^{-1}. The result showed characteristic of current versus the potential.

3.4.6 Rate capability

The rate capability of the full batteries (bare Zn||**δ**-MnO$_2$, GP@Zn||**δ**-MnO$_2$ and PANZ@GP@Zn||**δ**-MnO$_2$) were carried out at current densities of 50 mA g^{-1}, 100 mA g^{-1}, 200 mA g^{-1}, 500 mA g^{-1} and 200 mA g^{-1}, respectively. The current density and specific capacity values of the electrodes were normalized to the mass of **δ**-MnO$_2$. The result showed the discharge specific capacity versus cycle number at various current densities.

Chapter IV

Results and Discussion

The cross-section field emission scanning electron microscopy (FE-SEM) images of PANZ@GP@Zn as shown in Figure 4.1 was used to inspect the morphologies of the anode surface and thickness of coating layer before charging/discharging process, in which thickness of the PANZ layer and the graphite layer were 7-9 μm and approximately 93 μm, respectively.
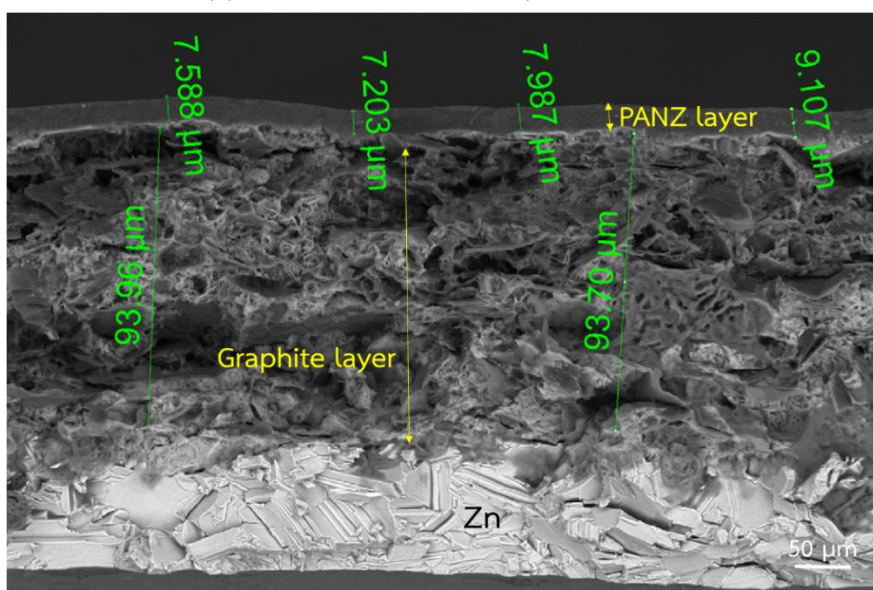

Figure 4.1 Cross-section view FE-SEM image of PAN@GP@Zn electrode before charging/discharging process.

4.1 Impedance and Ionic conductivity of zinc anode
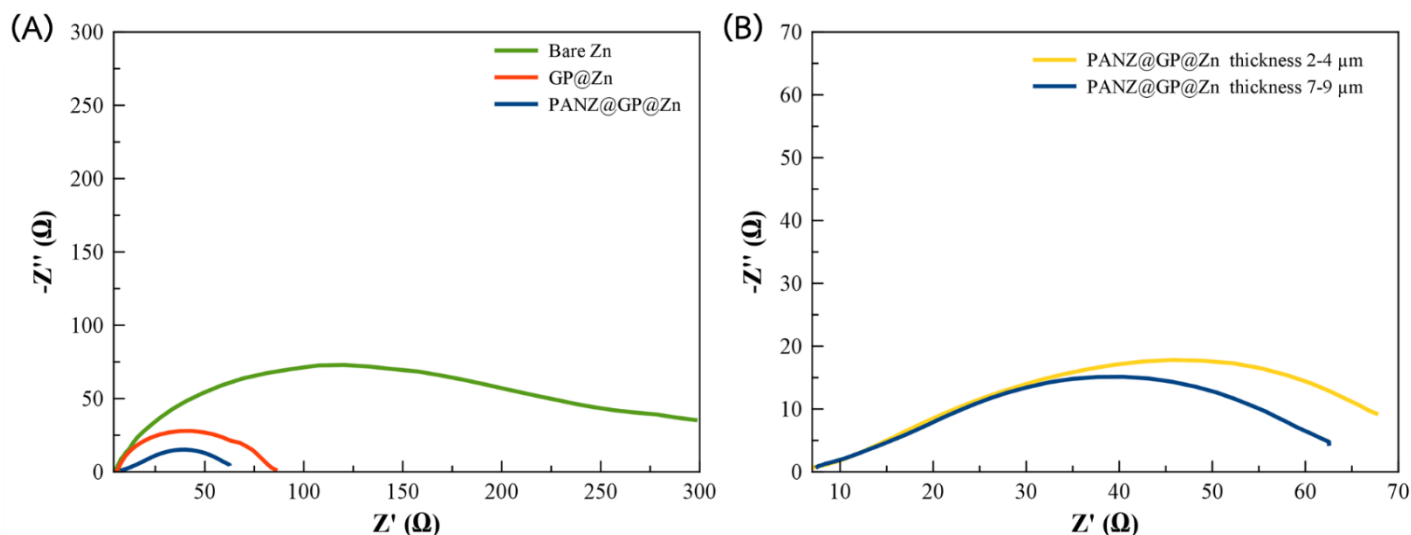
*Figure 4.2 Electrochemical impedance spectra (EIS) of symmetric cells with bare Zn,
GP@Zn and PANZ@GP@Zn anodes (A), PANZ@GP@Zn anodes at different thickness
of polymer layer (B) before cycling test.*

To test the impedance and ionic conductivity of zinc electrodes with bare Zn,
graphite coated zinc (GP@Zn) and zinc was coated with the PANZ and graphite
(PANZ@GP@Zn) in concentrated aqueous electrolyte of 2 M $ZnSO_4$. As shown in
Figure 4.2A, the Nyquist curves of impedance spectra of the different anodes before
cycling presented the PANZ interfacial coating layer (PANZ@GP@Zn) reduced the
impedance of the zinc anode more than the graphite layer (GP@Zn) and without
coating layer (bare Zn). The result showed that the PANZ@GP@Zn had the highest
ionic conductivity, which implied that the fast Zn^{2+} transport through the PANZ layer.
The PANZ@GP@Zn anodes at different thickness of polymer layer as shown in Figure
4.2B, compared to the PANZ@GP@Zn with polymer layer thickness 2-4 µm, the
PANZ@GP@Zn with polymer layer thickness 7-9 µm had lower impedance curve of
charge transfer at the electrode/electrolyte interface and Zn-ion transport through
SEI film, indicating the PANZ@GP@Zn with polymer layer thickness 7-9 µm had higher
ionic conductivity than thinner polymer layer. Thus, the PANZ@GP@Zn with polymer

layer thickness 7-9 μm was chosen for the stability of battery, the coulombic efficiency (CE) and rate capability test.

4.2 Anticorrosion capability
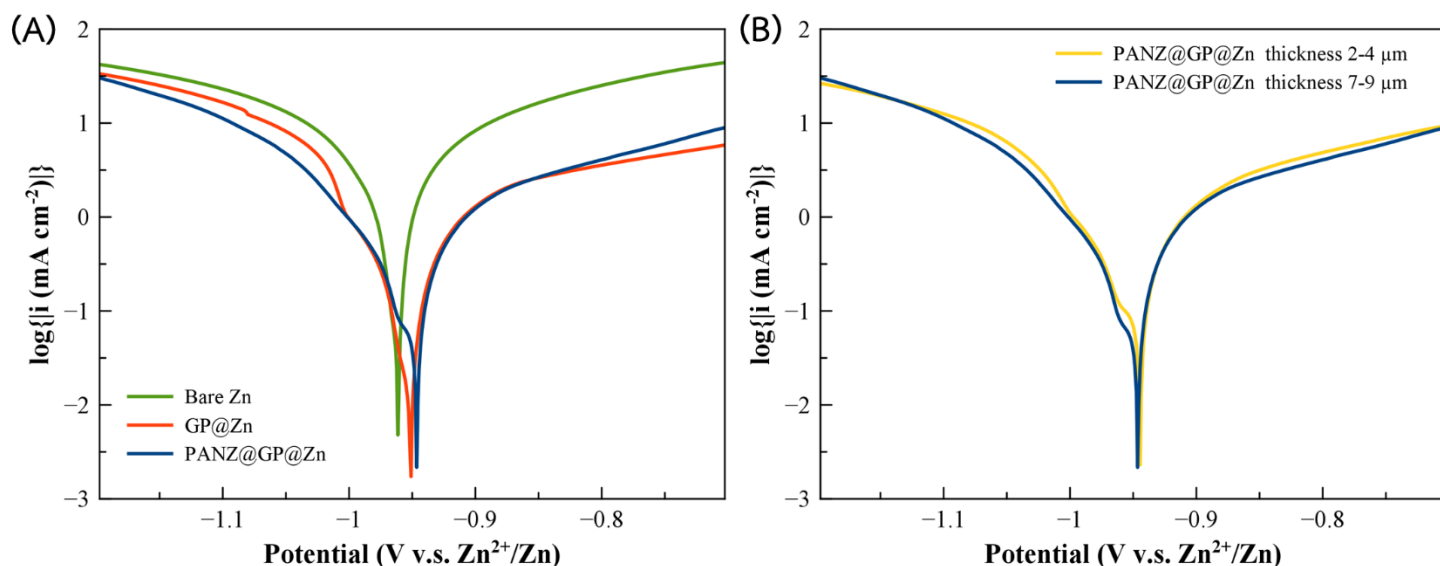
Figure 4.3 The Tafel curves of bare Zn, GP@Zn and PANZ@GP@Zn (A), PANZ@GP@Zn at different thickness of polymer layer (B) in 2 M ZnSO$_4$ electrolyte.

The anticorrosion capability of coating layer on anode and the effect of the PANZ coated graphite and graphite coated on the zinc corrosion were analyzed by Tafel curves in an electrolyte of 2 M ZnSO$_4$ as shown in Figure 4.3. Compared to the bare Zn, the corrosion potential of zinc which was coated with the PANZ and graphite (PANZ@GP@Zn) at polymer layer thickness 7-9 μm and zinc which was coated with graphite (GP@Zn) increase from -0.9613 V to -0.9465 V and from -0.9613 V to -0.9510 V, respectively as shown in Figure 4.3A. The result showed more positive corrosion potential that indicates less tendency of corrosion reactions and hydrogen evolution reaction [8], [18]. Moreover, the PANZ layer (PANZ@GP@Zn) also reduced the corrosion current. Thus, the polymer layer has lower corrosion rate. When compared graphite coated Zn (GP@Zn), the PANZ layer had the more positive corrosion potential, which indicated that the PANZ layer tends to be more corrosion

resistant than graphite coated zinc. To study the thickness of the PANZ layer affects the anticorrosion ability of the zinc anode. The PANZ layer coated zinc anode at polymer layer thickness 2-4 μm and 7-9 μm was considered as shown in Figure 4.3B. The Tafel curve of PANZ@GP@Zn at polymer layer thickness 2-4 μm showed slightly more positive corrosion potential than PANZ@GP@Zn at polymer layer thickness 7-9 μm.

4.3 The cycle performance and stability of battery

4.3.1 The morphologies of zinc anodes

The morphologies of the bare Zn, GP@Zn and PANZ@GP@Zn electrodes before cycling and after 100 cycles was examined by FE-SEM (Figure 4.4). The FE-SEM images displayed the morphologies of the electrodes before cycling. The morphology of bare Zn in Figure 4.4A had quite smooth surface but some area still had rough surface. The morphology of graphite coated Zn (GP@Zn) as shown in Figure 4.4B showed the rough surface with considerable voids. The morphology of the PANZ layer and graphite coated Zn in Figure 4.4C showed micropores over the surface. However, after 100 charge/discharge cycles, the bare Zn cell was covered all over by corrosion pits, Zn dendrites as shown in Figure 4.4D, 4.5. The formation of dendrites is also the problem of Zn anode because inactive dendrite can block the transfer of ions and slow the ion diffusion process, while the GP@Zn cell in Figure 4.4E showed zinc deposit over the surface of graphite layer caused by zinc migrated from interface between the zinc anode and the graphite layer onto the graphite layer due to good electronic conductivity of graphite particles. In contrast, the PANZ@GP@Zn cell as shown in Figure 4.4F found slightly zinc on the surface of polymer layer caused by zinc deposited between the graphite surface and the PANZ layer because the polymer layer's relatively thin thickness of 7-9 μm (Figure 4.1), some zinc can penetrate through its pores. Although the PANZ layer cannot prevent zinc migration onto the carbon layer, it can reduce zinc deposition over the anode surface when compared with the carbon layer.
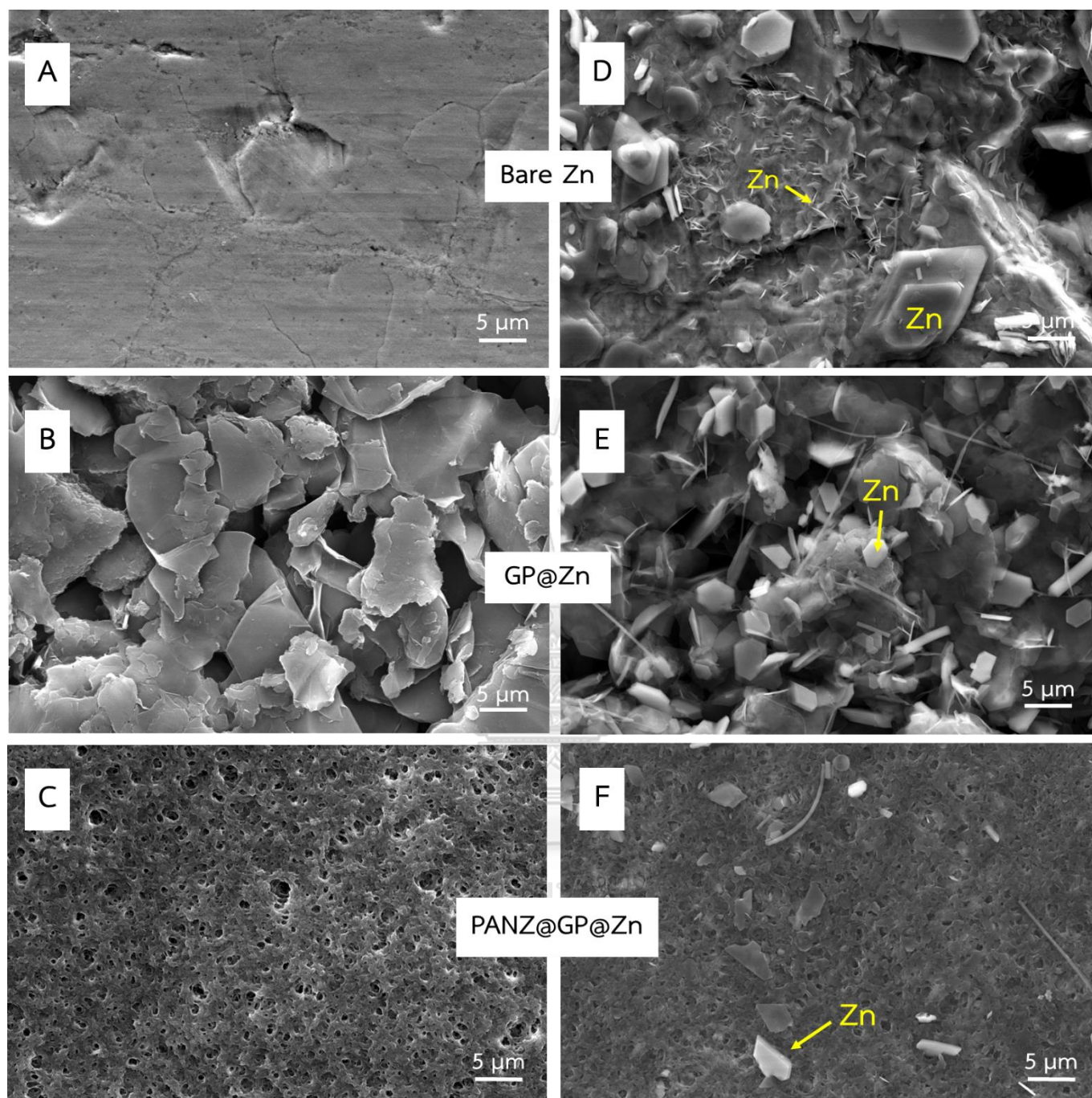
Figure 4.4 Top view FE-SEM images of Zn electrode with bare Zn, GP@Zn and PANZ@GP@Zn cells (A, B, C) before the cycling test, (D, E, F) after 100 cycles at a current density of 1 mA cm^{-2} with 1 mAh cm^{-2}.
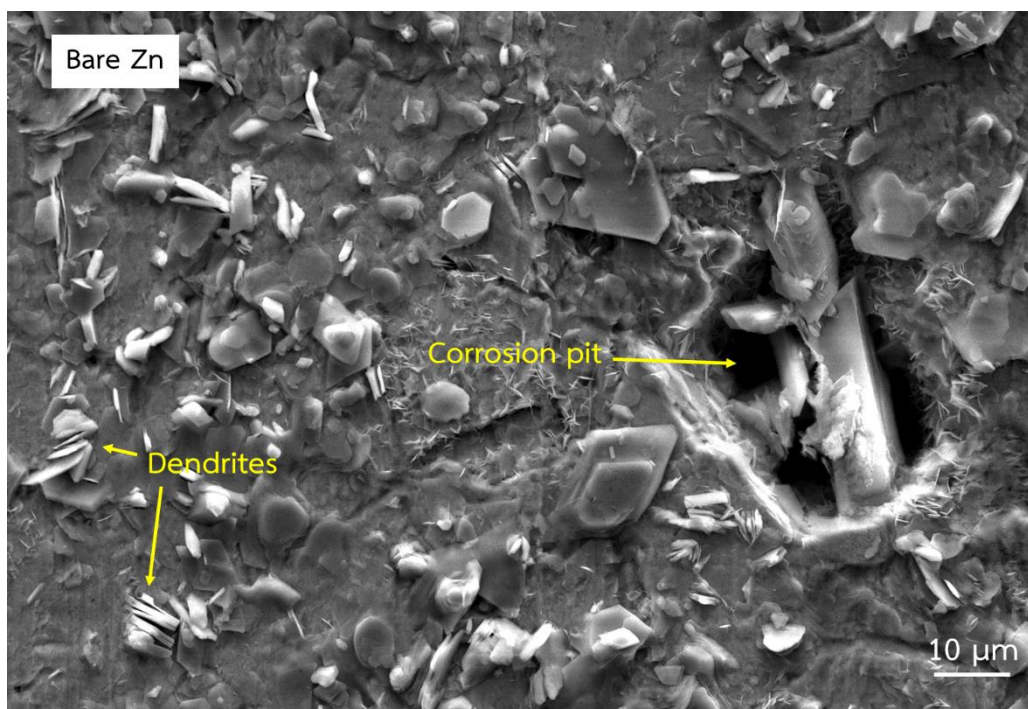
Figure 4.5 Top view FE-SEM images of bare Zn electrode after 100 cycles at a current density of 1 mA cm^{-2} with a fixed capacity of 1 mAh cm^{-2}.
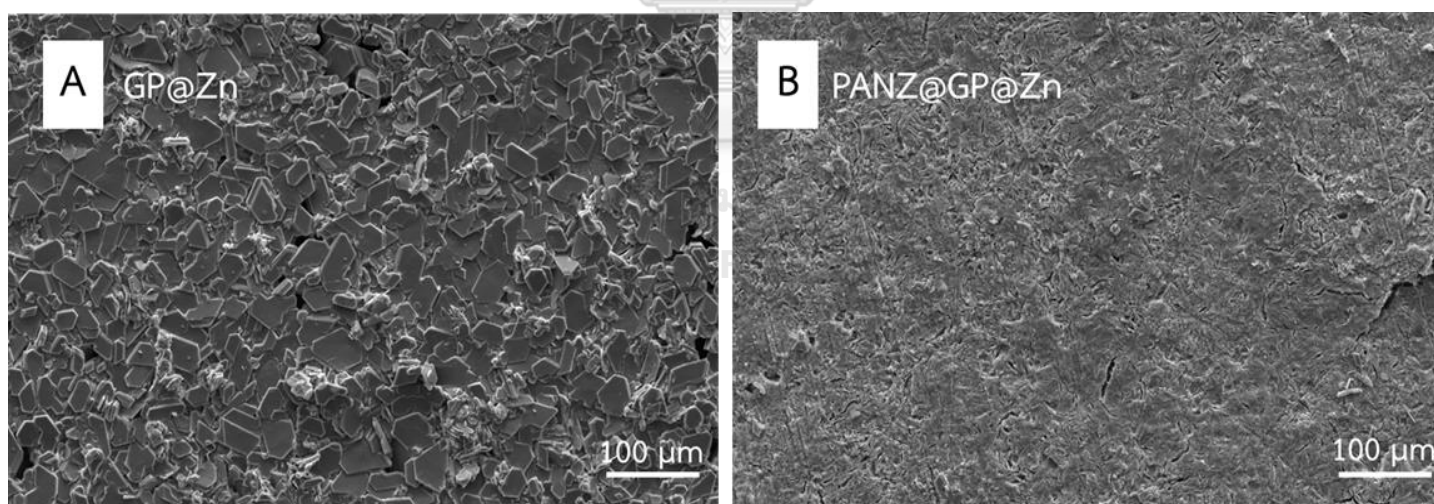
Figure 4.6 FE-SEM image of zinc deposition at interfacial between Zn foil and the coating layer of GP@Zn (A), PANZ@GP@Zn (B) symmetrical cells.

After charging process of ZIBs, zinc was deposited at interface between zinc foil and the coating layer. As shown in Figure 4.6, The PANZ and graphite coating layer on PANZ@GP@Zn and GP@Zn were peeled off to reveal the morphology change of the zinc metal, and the FE-SEM image in Figure 4.6A displayed interface of GP@Zn which had slightly uniform deposition of Zn on the zinc electrode surface but also had not uniform deposition of Zn in some areas. In contrast, interface of PANZ@GP@Zn had dense layer and uniform deposition of Zn on the zinc electrode surface, consequently inhibiting dendrite formation because microchannels in the polymer network has the complexation effect between $Zn^{2+}$ and the cyano groups (–CN), which can facilitate the uniform transport of dissolved Zn^{2+} in the PANZ layer and drives the uniform electrodeposition of zinc metal as shown in Figure 4.6B.
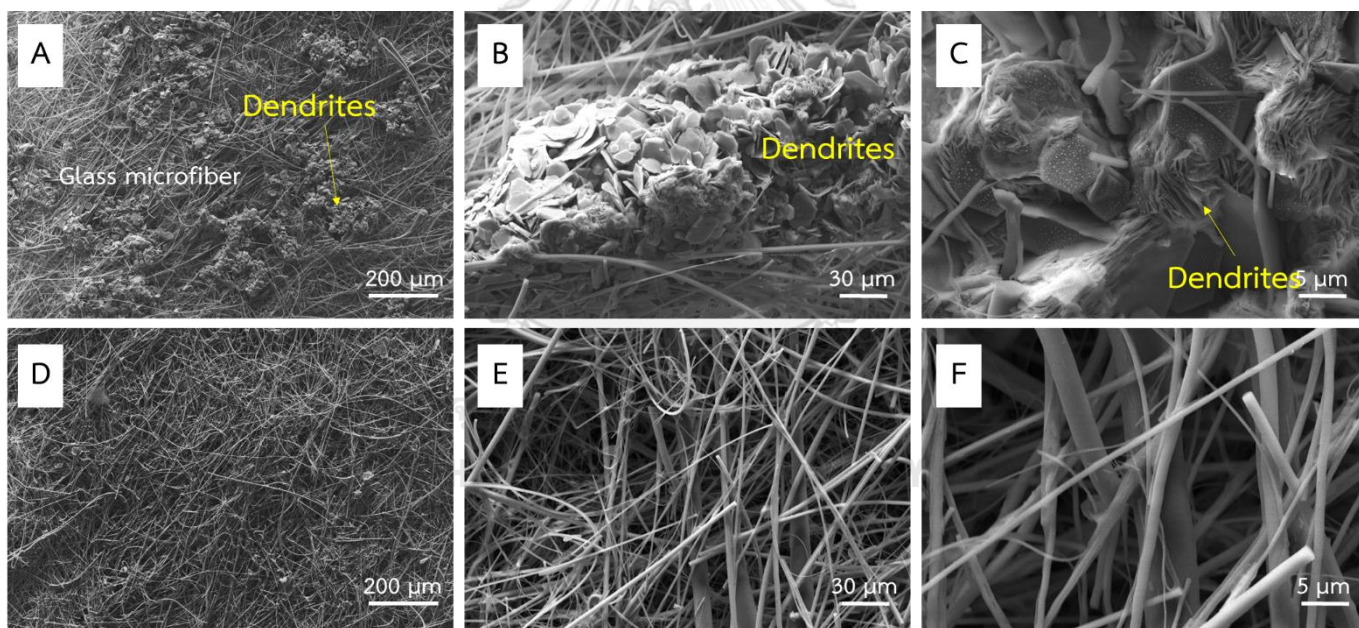
Figure 4.7 FE-SEM images of glass microfiber separator disassembled from the symmetrical cell with GP@Zn electrode (A, B, C), PANZ@GP@Zn electrode (D, E, F) after 100 cycles at a current density of 1 mA cm^{-2} with 1 mAh cm^{-2}.
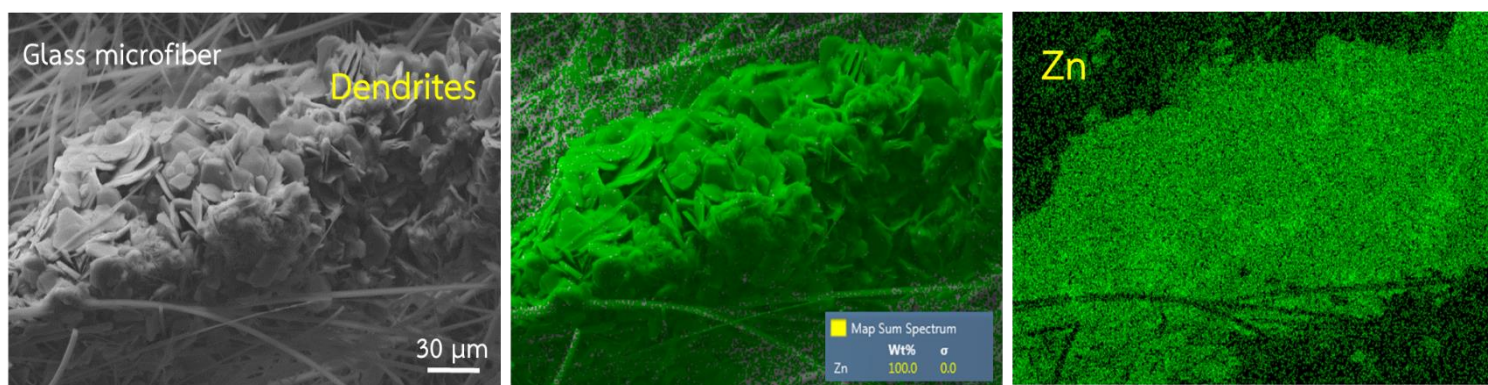
Figure 4.8 EDS images and corresponding Zn element maps of separator pierced by dendrites from the symmetric cell with GP@Zn electrode after 100 cycles at a current density of 1 mA cm^{-2} with 1 mAh cm^{-2}.

The morphologies of glass microfiber separator disassembled from the symmetrical cell with GP@Zn electrode, PANZ@GP@Zn electrode after 100 cycles at a current density of 1 mA cm^{-2} with 1 mAh cm^{-2}. As shown in Figure 4.7D, E and F, the glass microfiber separator of PANZ@GP@Zn electrode showed glass microfiber without dendrite. The separator of GP@Zn electrode as in Figure 4.7A and C showed flake-shaped dendrites spread on the separator surface and the separator pierced by dendrites as shown in Figure 4.7B, leading to the internal short circuit in the cell. The energy-dispersive X-ray spectroscopy (EDS) of the Zn elements confirmed the dendrites pierced through the separator as shown in Figure 4.8.

4.3.2 The stability of battery

Figure 4.9 The cycling performance of symmetrical Zn cells with bare Zn, GP@Zn and PANZ@GP@Zn at a current density of 1 mA cm^{-2} with 1 mAh cm^{-2}.

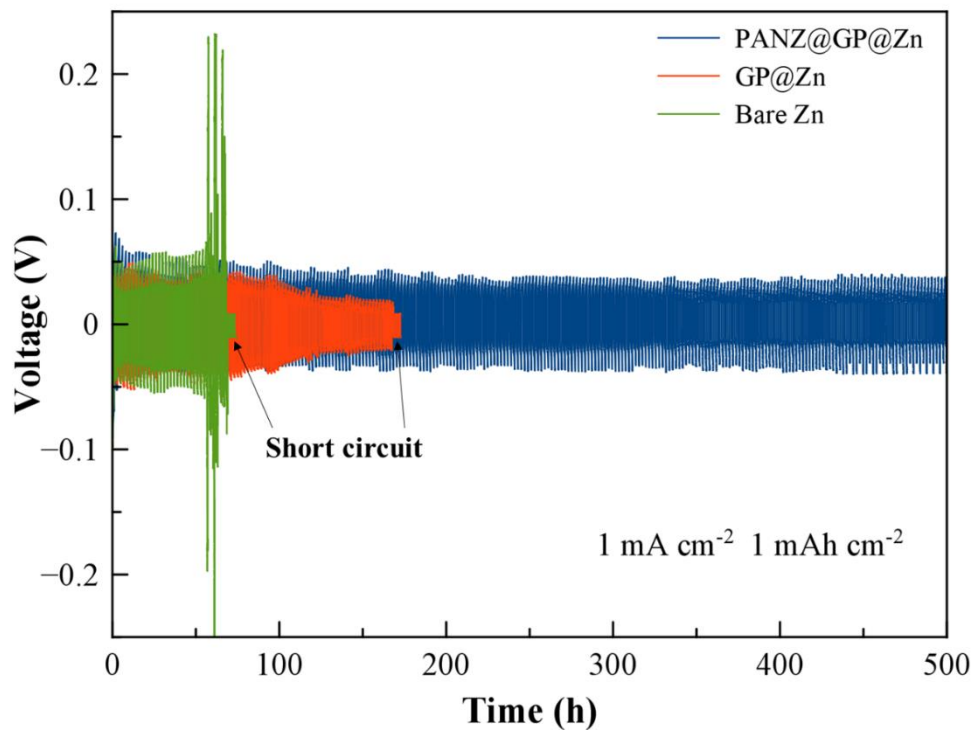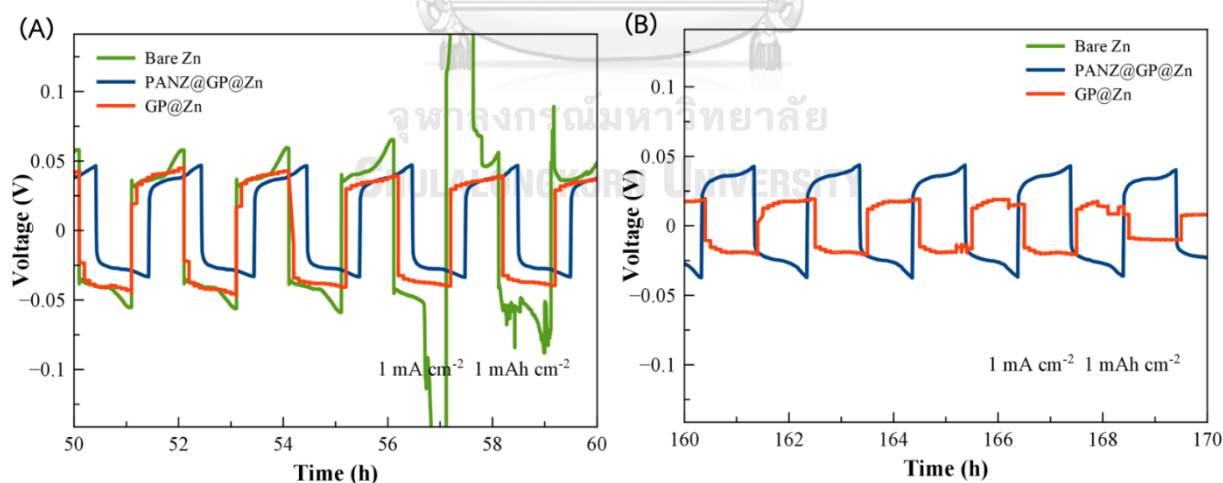*Figure 4.10 The cycling performance of symmetrical Zn cells with bare Zn, GP@Zn and PANZ@GP@Zn at a current density of 1 mA cm^{-2} with 1 mAh cm^{-2} (A) between 25 to 30 cycles (50 to 60 hours), (B) between 80 to 85 cycles (160 to 170 hours).*

To evaluate the stability of symmetrical Zn cells with bare Zn, GP@Zn and PANZ@GP@Zn were assembled with concentrated aqueous electrolyte of 2 M $ZnSO_4$ and inspected with the galvanostatic cycling test. After 25 cycles (50 hours) at a current density of 1 mA cm^{-2} with a capacity of 1 mAh cm^{-2} as shown in Figure 4.9, the cycling curve of bare Zn cell showed serious fluctuation and short circuit at 35 cycles (70 hours), which was inhomogeneous current distribution caused by the surface morphologies of bare Zn change during the charging/discharging processes of ZIBs due to dendrites, corrosion pits, hydrogen gas bubble found on the surface of bare Zn (Figure 4.4D, 4.5) [5], [7]. On the other hand, the cycling curve of graphite coated Zn cell (GP@Zn) demonstrated more stable cycling than bare Zn but the GP@Zn had reduced polarization voltage from 0.0390 V to 0.0186 V (Figure 4.10B), which implied that the GP@Zn had migrated of Zn ions from the interface surface between Zn foil and the graphite layer to redeposition over the surface of graphite owing to good electronic conductivity of graphite particles [3]. Thus, the cycling curve of GP@Zn exhibited short circuit at 85 cycles (170 hours) because glass microfiber separator pierced by dendrites. In contrast, the PANZ@GP@Zn showed very stable curves during 250 cycles (500 hours) caused by the PANZ layer (Polyacrylonitrile with zinc trifluoromethanesulfonate) as ASEI which can regulate zinc ion distribution and uniform nucleation sites for zinc deposition on the anode surface (Figure 4.6B), leading to suppressing side reactions and high cycling stability of ZIBs [8]. The PANZ@GP@Zn can also stably run until 543 hours with overpotential below 0.05 V before short circuit. Therefore, the PANZ@GP@Zn cell has the most stability cycling and long-term cycling than bare Zn and GP@Zn cell.

4.4 The Coulombic efficiency (CE)
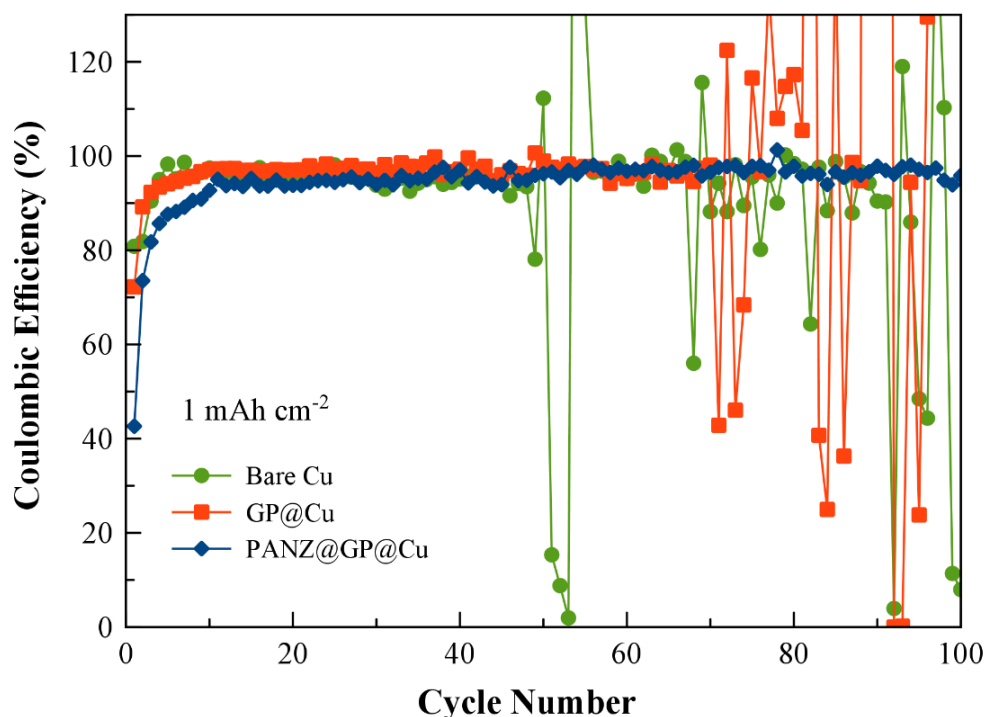
Figure 4.11 The coulombic efficiency (CE) of Zn plating/stripping in the bare Cu||bare Zn, GP@Cu||GP@Zn and PANZ@GP@Cu||PANZ@GP@Zn half cells.

To investigate the effect of the PANZ coating layer and graphite layer on the coulombic efficiency (CE) of the reversibility of the Zn/Zn^{2+} process. During each cycling, Zn was dissolved from the Zn metal as cathode and deposits onto the Cu as anode. To study of CE, a PANZ coating layer and graphite layer was coated on copper foil (PANZ@GP@Cu) then tested half cells (PANZ@GP@Cu||PANZ@GP@Zn) and compared with bare Cu||bare Zn and GP@Cu||GP@Zn anodes. The test was carried out by plating zinc (fixed areal capacity: 1 mAh cm^{-2}) onto the Cu, GP@Cu and PANZ@GP@Cu substrate and then stripping to -0.4 V. As displayed in Figure 4.11, fluctuant voltage signals during Zn plating/stripping were observed with the bare Cu and the GP@Cu electrode because of side reactions such as dendrite formation, hydrogen evolution reaction (HER) and corrosion. On the other hand, the PANZ@GP @Cu cell presented a very stable coulombic efficiency (CE) over 100 cycles (200 h), maintaining an average CE of 98.11% from cycle 10 (90.57%) to 100 (97.72%).

4.5 Rate capability
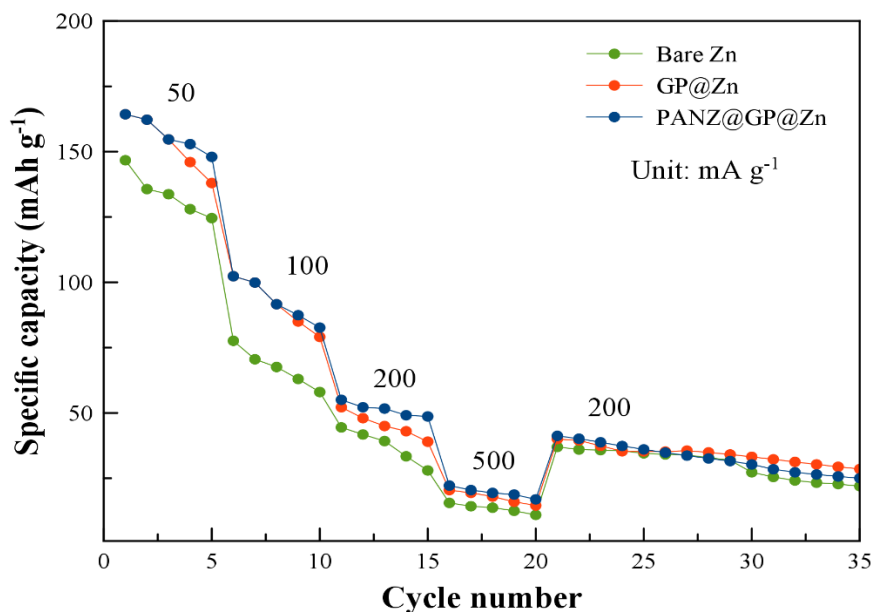
Figure 4.12 Rate capability of full batteries from 50, 100, 200, 500 and 200 mA g^{-1} based on the mass of δ-MnO$_2$.

Full prototype cells were assembled to prove the practical application of our electrode. One of the most commonly used cathodes for aqueous ZIBs was delta-MnO$_2$ (δ-MnO$_2$), the δ-MnO$_2$ was investigated to further evaluate the impact of the PANZ coating layer and graphite layer on the electrochemical performance of full batteries consisting of bare Zn‖δ-MnO$_2$, GP@Zn‖δ-MnO$_2$ and PANZ@GP@Zn‖δ-MnO$_2$ cells. The cells were charged/discharged in 2 M ZnSO$_4$ + 0.5 M MnSO$_4$ electrolyte, and MnSO$_4$ additive was used to suppress the dissolution of Mn^{2+} from the cathode [18], [19]. The rate capability of the bare Zn‖δ-MnO$_2$, GP@Zn‖δ-MnO$_2$ and PANZ@GP@Zn‖δ-MnO$_2$ batteries were also tested at various current densities ranging from 50, 100, 200, 500 and 200 mA g^{-1}. As shown in Figure 4.12, the rate capability of the PANZ@GP@Zn‖δ-MnO$_2$ was better than that of GP@Zn‖δ-MnO$_2$ and Zn‖δ-MnO$_2$,

which implies that PANZ@GP@Zn can reduce the fading of capacity than other anodes.

Chapter V

Conclusion

In this work, polyacrylonitrile with zinc trifluoromethanesulfonate was used as ASEI on the graphite (GP) layer onto the zinc anode (PANZ@GP@Zn). It was compared with the anode having graphite coated layers (GP@Zn) and bare zinc anode in rechargeable aqueous zinc-ion batteries (ZIBs). The PANZ@GP@Zn with polymer layer thickness 7-9 μm can reduce the impedance of the zinc anode more than the graphite layer, which has the highest ionic conductivity. At the same time, The PANZ@GP@Zn also has more positive corrosion potential that indicates less tendency of corrosion reactions and hydrogen evolution reaction. The long-term cycling performance and cycling stability of the zinc anodes at a current density of 1 mA cm^{-2} with fixed capacity of 1 mAh cm^{-2}. The PANZ@GP@Zn has the higher cycling stability and long-term durability than bare Zn and GP@Zn cell caused by the PANZ layer as ASEI can regulate zinc ion distribution and uniform nucleation sites for zinc deposition on the anode surface. Moreover, the effect of the PANZ coating layer on the coulombic efficiency (CE) has more stable coulombic efficiency (CE) over 100 cycles (200 h) than other anodes. However, the morphology of PANZ@GP@Zn after 100 cycles at a current density of 1 mA cm^{-2} shows slightly zinc on the surface of polymer layer caused by zinc deposited between the graphite surface and the PANZ layer because zinc migrates and redeposits over the surface of graphite owing to good electronic conductivity then some zinc can penetrate through micropores of polymer. Although the PANZ layer cannot prevent zinc migration onto the carbon layer, it can reduce zinc deposition over the anode surface when compared with the carbon layer, indicating that it can improve the battery's life. To identify the practical application, the rate capability of the PANZ@GP@Zn||δ-MnO$_2$ is better than other anodes, which implies that the PANZ@GP@Zn is suitable anode that can reduce the fading of capacity. Therefore, the PANZ@GP@Zn can increase ionic conductivity and suppress side reactions, leading to high cycling stability of ZIBs and extending the battery's life.
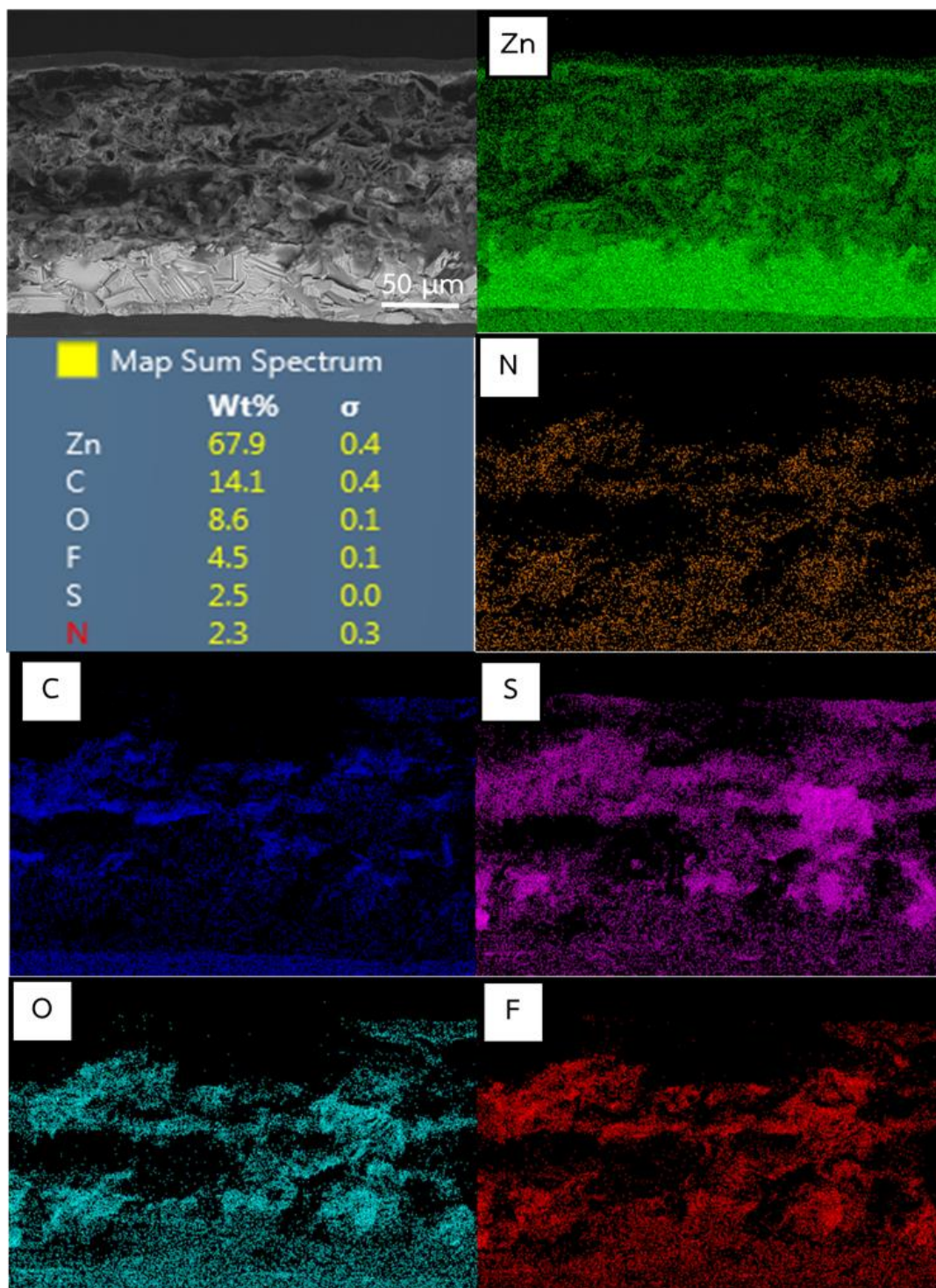
Appendix

Figure A1 EDS images and corresponding Zn, C, O, F, S and N element maps of cross-section view FE-SEM image of PAN@GP@Zn electrode before charging/discharging process.
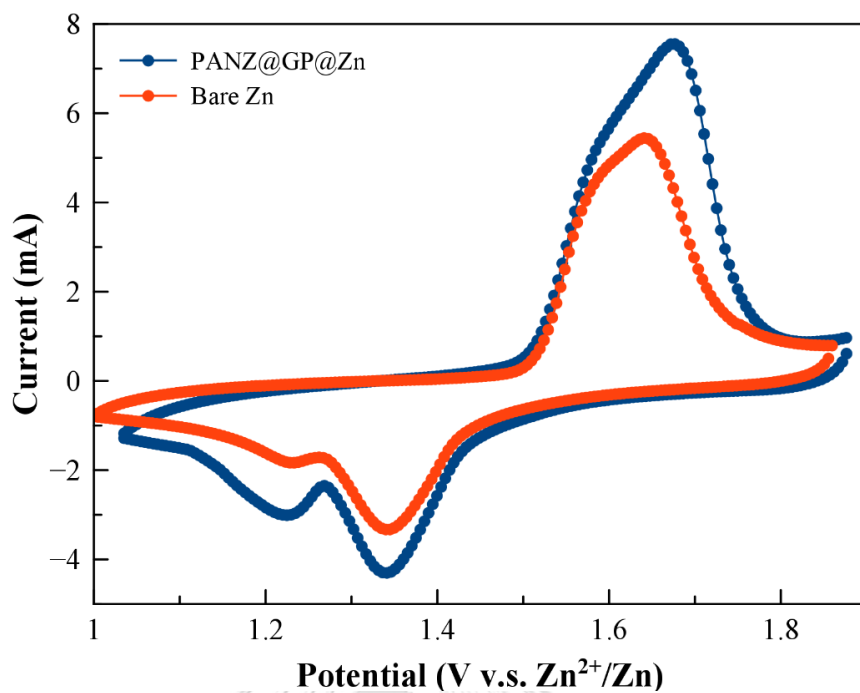
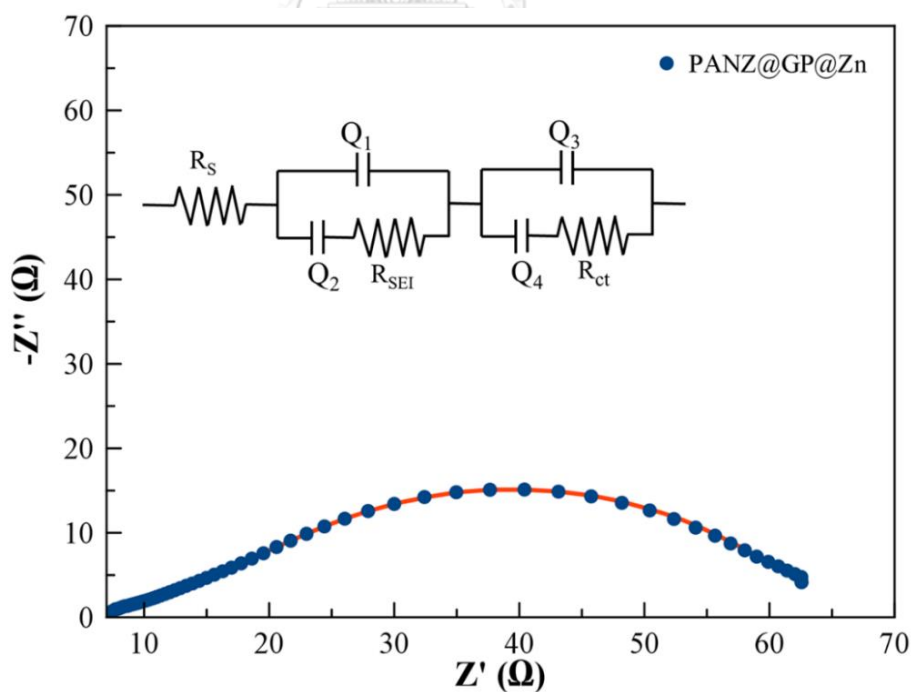*Figure A2 Cyclic voltammetry of full batteries, scan rate 0.3 mV s^{-1}.*

Figure A3 EIS of the PANZ@GP@Zn electrodes before cycling tests and match model.

Table 2 Different zinc anode modification methods and the corresponding electrochemistry performance.

No.	Zinc anodes	Current density (mA cm^{-2})	Areal capacity (mAh cm^{-2})	Worked time (h)	Zn foil thickness (mm)	Total capacity (mAh cm^{-2})	Calculate DOD (%)	References
1	Gelatin@Zn	1	1	4000	0.1	29.275	3.416	[20]
2	BaTiO$_3$@Zn	1	1	4000	0.05	58.55	1.708	[21]
3	ZnSe@Zn	1	1	1500	0.1	58.55	1.708	[22]
4	rGO@Zn	1	1	1200	0.15	585.5	0.2	[23]
5	Pitted Zn surface texture	1	1	1000	0.1	58.55	1.708	[24]
6	ZnF$_2$@Zn	1	1	800	0.1	58.55	1.708	[25]
7	This work	1	1	543	0.05	29.275	3.416	
8	ALD-Al$_2$O$_3$@Zn	1	1	500	0.2	117.1	0.854	[26]
9	Faceted TiO$_2$@Zn	1	1	460	0.03	17.565	5.693	[27]
10	C@Zn (ZIF-8 pyrolysis)	1	1	400	0.25	146.37	0.683	[28]
11	AC@Zn	1	1	200	0.08	46.84	2.135	[5]

The ranking is determined by how long the battery has been in use under the same conditions (a current density of 1 mA cm^{-2} with areal capacity of 1 mAh cm^{-2}). However, the depth of discharge (DOD) is a factor that affects the battery's working time. Therefore, %DOD should also be considered. The term "depth of discharge" (DOD) describes how much charge is cycled into and out of the battery during a specific cycle. It is represented as a percentage of the battery's total capacity. A

battery discharges at a high rate when it releases a lot of energy in a short period of time. Deep discharging (high %DOD) can drastically shorten battery life.

$$\% \text{ DOD} = \frac{test\ areal\ capacity}{total\ capacity} \times 100\%$$

Total capacity = Foil thickness (cm) ×   Theoretical capacity of Zn*

* Theoretical capacity of Zn is 5855 mAh cm^{-3} [17]

จุฬาลงกรณ์มหาวิทยาลัย
CHULALONGKORN UNIVERSITY

REFERENCES

1. Yi, Z., et al., *Strategies for the stabilization of Zn metal anodes for Zn‑ion batteries.* Advanced Energy Materials, 2021. **11**(1): p. 2003065.

2. Du, W., et al., *Challenges in the material and structural design of zinc anode towards high-performance aqueous zinc-ion batteries.* Energy & Environmental Science, 2020. **13**(10): p. 3330-3360.

3. Li, C., et al., *Issues and future perspective on zinc metal anode for rechargeable aqueous zinc‑ion batteries.* Energy & Environmental Materials, 2020. **3**(2): p. 146-159.

4. Bayaguud, A., Y. Fu, and C. Zhu, *Interfacial parasitic reactions of zinc anodes in zinc ion batteries: underestimated corrosion and hydrogen evolution reactions and their suppression strategies.* Journal of Energy Chemistry, 2022. **64**: p. 246-262.

5. Li, W., et al., *Advanced low-cost, high-voltage, long-life aqueous hybrid sodium/zinc batteries enabled by a dendrite-free zinc anode and concentrated electrolyte.* ACS applied materials & interfaces, 2018. **10**(26): p. 22059-22066.

6. Tao, H., et al., *Effect of adding various carbon additives to porous zinc anode in rechargeable hybrid aqueous battery.* Journal of Alloys and Compounds, 2016. **658**: p. 119-124.

7. Li, Z., et al., *Pencil drawing stable interface for reversible and durable aqueous zinc‑ion batteries.* Advanced Functional Materials, 2021. **31**(4): p. 2006495.

8. Chen, P., et al., *An Artificial Polyacrylonitrile Coating Layer Confining Zinc Dendrite Growth for Highly Reversible Aqueous Zinc‑Based Batteries.* Advanced Science, 2021. **8**(11): p. 2100309.

9. Chen, P., et al., *An integrated configuration with robust interfacial contact for durable and flexible zinc ion batteries.* Nano Energy, 2020. **74**: p. 104905.

10. Lorandi, F., et al., *Comparative performance of ex situ artificial solid electrolyte interphases for Li metal batteries with liquid electrolytes.* Iscience, 2021. **24**(6): p. 102578.

11.   He, P., et al., *Building better zinc-ion batteries: a materials perspective.*
      EnergyChem, 2019. **1**(3): p. 100022.

12.   Yang, J., et al., *Zinc Anode for Mild Aqueous Zinc-Ion Batteries: Challenges,
      Strategies, and Perspectives.* Nano-micro letters, 2022. **14**(1): p. 1-47.

13.   Wu, C., et al., *Dendrite-free Zn anodes enabled by functional nitrogen-doped
      carbon protective layers for aqueous zinc-ion batteries.* Dalton Transactions,
      2020. **49**(48): p. 17629-17634.

14.   Li, H., et al., *Enhancement on cycle performance of Zn anodes by activated
      carbon modification for neutral rechargeable zinc ion batteries.* Journal of the
      Electrochemical Society, 2015. **162**(8): p. A1439.

15.   Barnes, K. *What is Acrylonitrile? - Uses & Properties*. [cited 2022 19]; Available
      from: https://study.com/academy/lesson/what-is-acrylonitrile-uses-
      properties.html.

16.   KGaA, M. [cited 2022 19]; Available from:
      https://www.sigmaaldrich.com/TH/en/product/aldrich/290068.

17.   Hoang Huy, V.P., L.T. Hieu, and J. Hur, *Zn Metal Anodes for Zn-Ion Batteries in
      Mild Aqueous Electrolytes: Challenges and Strategies.* Nanomaterials, 2021.
      11(10): p. 2746.

18.   Zhao, Z., et al., *Long-life and deeply rechargeable aqueous Zn anodes
      enabled by a multifunctional brightener-inspired interphase.* Energy &
      Environmental Science, 2019. **12**(6): p. 1938-1949.

19.   Qiu, C., et al., *The function of Mn2+ additive in aqueous electrolyte for Zn/δ-
      MnO2 battery.* Electrochimica Acta, 2020. **351**: p. 136445.

20.   Shin, J., et al., *Highly reversible, grain‐directed zinc deposition in aqueous zinc
      ion batteries.* Advanced Energy Materials, 2021. **11**(39): p. 2100676.

21.   Zou, P., et al., *Ultrahigh‐Rate and Long‐Life Zinc–Metal Anodes Enabled by
      Self‐Accelerated Cation Migration.* Advanced Energy Materials, 2021. **11**(31): p.
      2100982.

22.   Zhang, L., et al., *Eliminating dendrites and side reactions via a multifunctional
      znse protective layer toward advanced aqueous Zn metal batteries.* Advanced

Functional Materials, 2021. **31**(26): p. 2100186.

23. Xia, A., et al., *Graphene oxide spontaneous reduction and self-assembly on the zinc metal surface enabling a dendrite-free anode for long-life zinc rechargeable aqueous batteries.* Applied Surface Science, 2019. **481**: p. 852-859.

24. Xu, Y., et al., *A self-preserving pitted texture enables reversible topographic evolution and cycling on Zn metal anodes.* Journal of Materials Chemistry A, 2021. **9**(45): p. 25495-25501.

25. Yang, Y., et al., *Synergistic manipulation of Zn2+ ion flux and desolvation effect enabled by anodic growth of a 3D ZnF2 matrix for long‑lifespan and dendrite‑free Zn metal anodes.* Advanced Materials, 2021. **33**(11): p. 2007388.

26. He, H., et al., *Highly stable Zn metal anodes enabled by atomic layer deposited Al 2 O 3 coating for aqueous zinc-ion batteries.* Journal of materials chemistry A, 2020. **8**(16): p. 7836-7846.

27. Zhang, Q., et al., *Revealing the role of crystal orientation of protective layers for stable zinc anode.* Nature communications, 2020. **11**(1): p. 1-7.

28. Yuksel, R., et al., *Metal‑organic framework integrated anodes for aqueous zinc‑ion batteries.* Advanced Energy Materials, 2020. **10**(16): p. 1904215.

จุฬาลงกรณ์มหาวิทยาลัย
CHULALONGKORN UNIVERSITY

VITA

NAME	Nutchaya Muangplod
DATE OF BIRTH	10 July 1997
PLACE OF BIRTH	Nonthaburi, Thailand
INSTITUTIONS ATTENDED	B.S. Industrial Chemistry Faculty of science at Kasetsart University
HOME ADDRESS	40, Thasai Subdistrict, Mueang Nonthaburi District, Nonthaburi 11000

จุฬาลงกรณ์มหาวิทยาลัย

CHULALONGKORN UNIVERSITY